Optimal torque control of permanent magnet synchronous machines using magnetic equivalent circuits

authored by **W. Kemmetmüller, D. Faustner, and A. Kugi**

and published in *Mechatronics*.

ACIN

Optimal Torque Control of Permanent Magnet Synchronous Machines Using Magnetic Equivalent Circuits

Wolfgang Kemmetmüller[a,*], David Faustner, Andreas Kugi[a]

[a]*Automation and Control Institute, Vienna University of Technology, Gusshausstr. 27-29, Vienna, Austria*

Abstract

In recent years, permanent magnet synchronous machines (PSMs) are often designed in a mechatronic way to obtain e.g. special torque characteristics at zero currents or maximum efficiency. These designs are often characterized by a pronounced magnetic saturation and non-sinusoidal properties. This paper describes the optimal torque control of such PSMs utilizing a magnetic equivalent circuit (MEC) model. In contrast to approaches based on fundamental wave models (dq0-models), which utilize the Blondel-Park transformation and typically consider saturation and non-sinusoidal characteristics only in a heuristic way, MEC models allow to systematically account for these effects. Given the MEC model, optimal values for the coil currents are obtained from a constrained, nonlinear optimization problem, which can be efficiently solved by exploiting the special mathematical structure of the model. The results of the optimization are used in a flatness-based torque control strategy. The performance and practical feasibility of the proposed torque control concept are demonstrated by experiments on a test stand. Finally, it is shown that using this torque control in an outer angular speed control loop also proves to be beneficial.

Keywords: Optimal torque control, magnetic equivalent circuit, permanent magnet synchronous motor, flatness based control

1. Introduction

The accurate control of the torque is essential in many applications of permanent magnet synchronous machines (PSMs), which makes this topic an active field of research in recent years. The industrial standard to control PSMs is field oriented control (FOC), which is based on a fundamental wave model and the application of the Blondel-Park transformation, see, e.g., [1, 2]. A number of research papers have discussed the development of advanced (nonlinear) control strategies based on this model. E.g., [3–5] propose exact feedback linearization, [6–8] use backstepping control and passivity based methods are applied in [9–11] to the control of PSMs. Furthermore, sliding mode control is examined in [12–14], model predictive control is used in [15–17] and direct torque control concepts can be found in [18–20]. These control strategies in general exhibit a good performance for PSMs and operating regions, which can be accurately described by a (magnetically linear) fundamental wave model (dq0-model).

For applications with high demands on torque, speed or position accuracy, it happens more often in recent years that motor designs are employed which do not satisfy the assumptions that have to be made for the derivation of classical dq0-models. In particular, fractional slot concentrated windings and rotors with interior permanent magnets are preferred by industry due to the simpler and cheaper construction. Moreover, to shape the torque characteristics especially for zero currents, inhomogeneous air gap geometries are frequently used in a mechatronic design approach. These constructions often yield pronounced nonsinusoidal (non-fundamental wave) characteristics of the back-emf and the inductances of the motor. Moreover, PSMs are often operated in a region, where significant saturation of the iron parts occurs.

Heuristic extensions of the dq0-model are typically proposed in literature to account for saturation and non-fundamental wave characteristics. E.g., the control strategies in [21–31] are based on an extension of the dq0-model by higher harmonics in the back emf, the inductances or the resulting torque. In these works, however, the influence of saturation and the resulting cogging or reluctance torque are not considered. Saturation is again incorporated into the dq0-model in a heuristic manner, see, e.g., [32–37].

The limitations of these approaches clearly result from the underlying dq0-model such that a more rigorous modeling approach is preferable. A magnetic equivalent circuit approach was described in [38, 39] for the modeling of PSMs with internal or surface mounted magnets. It was shown that an accurate description of the behavior of PSMs with non-fundamental wave characteristics and significant saturation can be achieved with this approach. Since the resulting models feature a limited model com-

*Corresponding author

Email addresses: kemmetmueller@acin.tuwien.ac.at (Wolfgang Kemmetmüller), (faustner,kugi)@acin.tuwien.ac.at (David Faustner, Andreas Kugi)

Post-print version of the article: W. Kemmetmüller, D. Faustner, and A. Kugi, "Optimal torque control of permanent magnet synchronous machines using magnetic equivalent circuits", *Mechatronics*, vol. 32, pp. 22–33, 2015. DOI: 10.1016/j.mechatronics.2015.10.007
The content of this post-print version is identical to the published paper but without the publisher's final layout or copy editing.

plexity, these models can be considered a good basis for the controller design.

In this work, the optimal torque control of PSMs which show both significant magnetic saturation and non-sinusoidal characteristics is considered. As a test case, a PSM with interior permanent magnets is used, which was designed for a rear steering system of a car. In this application, a motion of the PSM has to prevented in case of a failure of the power electronics. This is achieved by designing an inhomogeneous air gap geometry which results in a large cogging torque. This in turn prevents undesired rotation of the motor at zero currents. However, the significant non-sinusoidal behavior and saturation complicates the accurate torque control of such PSMs. The corresponding mathematical model is described in [38], which will serve as a basis for the controller design. The control strategy is based on the solution of a nonlinear, constrained optimization problem in combination with a flatness-based feedback control. In [40], also the optimal torque control of a PSM, which exhibits significant saturation, based on an MEC model is considered. For this surface magnet PSM it is, however, possible to accurately approximate the characteristic quantities like the flux linkage of the coils by means of fundamental wave components, with only their amplitudes and phase angles being nonlinear functions of the coil currents. It is demonstrated in [40] how the fundamental wave characteristics can be beneficially utilized to solve the resulting optimal control problem. The present work deals with the more general case containing both magnetic saturation and non-fundamental wave characteristics.

The paper is organized as follows: The mathematical model of [38] is briefly summarized in Section 2. In Section 3, the calculation of optimal currents is described, which is used in the flatness based control strategy outlined in Section 4. Measurement results of a test stand presented in Section 5 demonstrate the good control performance and the practical feasibility of the proposed control strategy. Finally, Section 6 elaborates the benefits of using the optimal torque control strategy in an outer control loop for the angular speed.

2. Mathematical Model

In [38], a general framework for the mathematical modeling of permanent magnet synchronous machines based on a magnetic equivalent circuit approach was derived. This approach was successfully applied to the modeling of both a surface-mounted PSM [39] and a PSM with internal magnets [38]. In this work, the same motor as in [38] will be used and therefore, the mathematical model derived in [38] serves as the basis for the development of the optimal torque control strategy.

The considered PSM with internal magnets comprises 12 coils and eight NdFeB-magnets. Figure 1 depicts the cross section of a quarter of the motor. As already briefly discussed in the introduction, the PSM is used in an automotive application, where it is absolutely important that

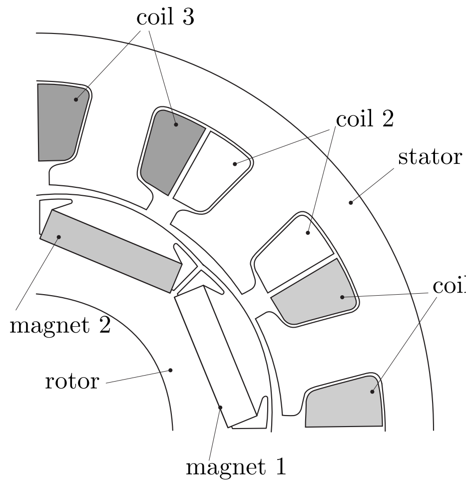

Figure 1: Cross section of the considered PSM [38].

no motion occurs in the case of e.g. a failure of the power electronics. This behavior is achieved by designing an inhomogeneous air gap which yields a large cogging torque, see Fig. 1. Moreover, this design also results in a non-sinusoidal back emf and a significant influence of saturation in the stator and rotor. As shown in [38], the motor can be accurately described by a (magnetically nonlinear) MEC, comprising magneto-motive force (mmf) sources describing the coils and the permanent magnets, and magnetically nonlinear or position dependent permeances describing the stator, the rotor, the air gap and the leakages. The mathematical equations of this MEC are derived using network theory, well established in the modeling of electric networks, see, e.g., [41–43]. For this purpose, a tree being composed of elements of the MEC and connecting all nodes of the network without forming a mesh is defined. The choice of this tree is arbitrary except for the fact that all mmf sources of the MEC have to be part of the tree. The remaining elements of the network form the corresponding co-tree of the network. The interconnection of the tree and co-tree elements, i.e. the topology of the MEC, is described by the incidence matrix $\bar{\mathbf{D}}^T = [\bar{\mathbf{D}}_c^T, \mathbf{D}_m^T, \mathbf{D}_g^T]$, where $\bar{\mathbf{D}}_c = \mathbf{N}_c \mathbf{D}_c$, with the winding matrix $\mathbf{N}_c = \mathrm{diag}[N_c, N_c, N_c]$ and the number N_c of windings per coil. Therein, $\mathbf{D}_c$ is the part of the incidence matrix which is related to the coils, $\mathbf{D}_m$ is related to the permanent magnets and $\mathbf{D}_g$ is related to the permeances of the tree. The permeances of the tree and co-tree are combined in the (diagonal) permeance matrices $\mathbf{G}_t$ and $\mathbf{G}_c$, respectively. Both, $\mathbf{G}_t$ and $\mathbf{G}_c$, are nonlinear functions of the rotor angle and the corresponding mmfs. The mathematical model of the MEC can then be formulated

Post-print version of the article: W. Kemmetmüller, D. Faustner, and A. Kugi, "Optimal torque control of permanent magnet synchronous machines using magnetic equivalent circuits", *Mechatronics*, vol. 32, pp. 22–33, 2015. DOI: 10.1016/j.mechatronics.2015.10.007
The content of this post-print version is identical to the published paper but without the publisher's final layout or copy editing.

in the form, see [38],

$$\frac{\mathrm{d}}{\mathrm{d}t}\boldsymbol{\psi}_c^I = -R_c\mathbf{i}_c^I + \left(\bar{\mathbf{D}}_c^I\right)^T\mathbf{v}_c \tag{1a}$$

$$\mathbf{0} = \mathbf{K}\begin{bmatrix}\mathbf{i}_c^I\\ \mathbf{u}_{tg}\end{bmatrix} - \begin{bmatrix}\boldsymbol{\psi}_c^I\\ \mathbf{0}\end{bmatrix} + \begin{bmatrix}\left(\bar{\mathbf{D}}_c^I\right)^T\bar{\mathbf{D}}_c\\ \mathbf{D}_g\end{bmatrix}\mathbf{G}_c\mathbf{D}_m^T\mathbf{u}_{tm} \tag{1b}$$

with

$$\mathbf{K} = \begin{bmatrix}(\bar{\mathbf{D}}_c^I)^T\bar{\mathbf{D}}_c\mathbf{G}_c\bar{\mathbf{D}}_c^T\mathbf{H}_1^I & (\bar{\mathbf{D}}_c^I)^T\bar{\mathbf{D}}_c\mathbf{G}_c\mathbf{D}_g^T\\ \mathbf{D}_g\mathbf{G}_c\bar{\mathbf{D}}_c^T\mathbf{H}_1^I & \mathbf{G}_t + \mathbf{D}_g\mathbf{G}_c\mathbf{D}_g^T\end{bmatrix}. \tag{2}$$

Therein, $\boldsymbol{\psi}_c^I$ is the vector of independent flux linkages, $\mathbf{i}_c^I$ is the corresponding vector of independent coil currents and R_c is the electrical resistance of a coil. The influence of the coil voltages $\mathbf{v}_c$ on the flux linkage is described by the matrix $\left(\bar{\mathbf{D}}_c^I\right)^T$, which reflects the magnetic connection of the coils. The set of algebraic equations (1b) describes the independent coil currents $\mathbf{i}_c^I$ and the mmfs $\mathbf{u}_{tg}$ of the permeances of the tree of the magnetic network as a function of the flux linkage $\boldsymbol{\psi}_c^I$ of the coils and the mmfs $\mathbf{u}_{tm}^T = [u_{ms}, -u_{ms}]$ of the permanent magnets, cf. [38]. Finally, $\mathbf{H}_1^I$ results from the inverse of a transformation matrix $\mathbf{T}_{1c}$, which has been used in [38] to eliminate the redundancies of the nonlinear algebraic equations, in the form $\mathbf{T}_{1c}^{-1} = [\mathbf{H}_1^\perp, \mathbf{H}_1^I]$.

The torque produced by the motor is given by

$$\tau = \frac{1}{2}p\Bigg(\mathbf{u}_{tg}^T\frac{\partial\mathbf{G}_t}{\partial\varphi}\mathbf{u}_{tg} + \left[(\mathbf{H}_1^I\mathbf{i}_c^I)^T, \mathbf{u}_{tm}^T, \mathbf{u}_{tg}^T\right]\bar{\mathbf{D}}\frac{\partial\mathbf{G}_c}{\partial\varphi}\bar{\mathbf{D}}^T\begin{bmatrix}\mathbf{H}_1^I\mathbf{i}_c^I\\ \mathbf{u}_{tm}\\ \mathbf{u}_{tg}\end{bmatrix}\Bigg), \tag{3}$$

with $p = 4$ being the number of pole-pairs of the motor.

A detailed derivation of this model and a evaluation of the model accuracy is given in [38], where a slightly different notation is used. It should be noted that the optimal control strategy developed in this manuscript can be applied to any motor construction which can be described by an MEC model of the form (1)-(3).

3. Calculation of optimal coil currents

The main goal of this work is to derive a control strategy which calculates the control inputs $\mathbf{v}_c$ in a way that the torque τ tracks a desired torque τ^*. As an intermediate step to this goal, the currents $\mathbf{i}_c$ are determined such that the resulting torque is equal to the desired torque for a given angle φ and the copper losses of the motor are minimal. In the following subsections, the calculation of optimal coil currents is discussed for the general magnetically nonlinear case, the magnetically linear case and the magnetically linear fundamental wave case.

3.1. Optimal currents: Magnetically nonlinear case

Calculating optimal currents for the magnetically and geometrically nonlinear case directly leads to a nonlinear optimization problem of the form

$$\min_{\mathbf{i}_c,\mathbf{u}_{tg}}\frac{1}{2}\left(\mathbf{i}_c\right)^T\mathbf{i}_c = \min_{\mathbf{i}_c^I,\mathbf{u}_{tg}}\frac{1}{2}\left(\mathbf{i}_c^I\right)^T\underbrace{\left(\mathbf{H}_1^I\right)^T\mathbf{H}_1^I}_{\mathbf{Q}}\mathbf{i}_c^I \tag{4}$$

subject to the nonlinear equality constraints

$$g = \tau(\mathbf{i}_c^I, \mathbf{u}_{tg}) - \tau^* = 0 \tag{5a}$$

$$\begin{aligned}\mathbf{h} = \left[\mathbf{D}_g\mathbf{G}_c\bar{\mathbf{D}}_c^T\mathbf{H}_1^I, \mathbf{G}_t + \mathbf{D}_g\mathbf{G}_c\mathbf{D}_g^T\right]\begin{bmatrix}\mathbf{i}_c^I\\ \mathbf{u}_{tg}\end{bmatrix}\\ + \mathbf{D}_g\mathbf{G}_c\mathbf{D}_m^T\mathbf{u}_{tm} = \mathbf{0},\end{aligned} \tag{5b}$$

with the positive definite matrix $\mathbf{Q} > 0$. Please note that by means of the constraint (5a) it is ensured that a solution is found which yields the desired torque τ^*. Moreover, (5b), which results from the second row of (1b), guarantees that the solution is compatible with the MEC-model of the motor.

To solve this optimization problem, the Lagrange function $\mathcal{L}$ is introduced in the form

$$\mathcal{L} = \frac{1}{2}\left(\mathbf{i}_c^I\right)^T\mathbf{Q}\mathbf{i}_c^I + \lambda g + \boldsymbol{\mu}^T\mathbf{h}, \tag{6}$$

with the Lagrange multipliers λ and $\boldsymbol{\mu}$. The first order necessary optimality condition states that the partial derivatives of $\mathcal{L}$ with respect to $\mathbf{i}_c^I$, $\mathbf{u}_{tg}$, λ and $\boldsymbol{\mu}$ must be equal to zero. In [44] and [45], a similar approach is chosen for the magnetically linear case, i.e. without taking into account the cogging torque, the reluctance torque and saturation.

The partial derivative of $\mathcal{L}$ with respect to $\mathbf{i}_c^I$ reads as

$$\begin{aligned}\left(\frac{\partial\mathcal{L}}{\partial\mathbf{i}_c^I}\right)^T &= \mathbf{Q}\mathbf{i}_c^I + \lambda p\left[\left(\mathbf{H}_1^I\right)^T, \mathbf{0}, \mathbf{0}\right]\bar{\mathbf{D}}\frac{\partial\mathbf{G}_c}{\partial\varphi}\bar{\mathbf{D}}^T\begin{bmatrix}\mathbf{H}_1^I\mathbf{i}_c^I\\ \mathbf{u}_{tm}\\ \mathbf{u}_{tg}\end{bmatrix}\\ &+\lambda\frac{p}{2}\left[\left(\mathbf{H}_1^I\mathbf{i}_c^I\right)^T, \mathbf{u}_{tm}^T, \mathbf{u}_{tg}^T\right]\bar{\mathbf{D}}\frac{\partial^2\mathbf{G}_c}{\partial\varphi\partial\mathbf{i}_c^I}\bar{\mathbf{D}}^T\begin{bmatrix}\mathbf{H}_1^I\mathbf{i}_c^I\\ \mathbf{u}_{tm}\\ \mathbf{u}_{tg}\end{bmatrix}\\ &+\left[\left(\mathbf{H}_1^I\mathbf{i}_c^I\right)^T, \mathbf{u}_{tm}^T, \mathbf{u}_{tg}^T\right]\bar{\mathbf{D}}\frac{\partial\mathbf{G}_c}{\partial\mathbf{i}_c^I}\mathbf{D}_g^T\boldsymbol{\mu} + \left(\mathbf{H}_1^I\right)^T\bar{\mathbf{D}}_c\mathbf{G}_c\mathbf{D}_g^T\boldsymbol{\mu}\end{aligned} \tag{7}$$

and the partial derivative with respect to $\mathbf{u}_{tg}$ can be formulated as given in (8). The partial derivatives with respect to λ and $\boldsymbol{\mu}$ of course yield the nonlinear equality constraints (5).

The solution of the constrained optimization problem (4), (5) is thus traced back to the solution of a system of nonlinear equations (5), (7) and (8). For a real-time implementation of the optimal control strategy, this set of equations must be solved in each sampling interval with sampling time T_s. Typically, T_s is in the order of 50 µs to 200 µs according to pulse-width-modulation (pwm) frequencies of 20 kHz to 5 kHz. Thus, high numeric efficiency

Post-print version of the article: W. Kemmetmüller, D. Faustner, and A. Kugi, "Optimal torque control of permanent magnet synchronous machines using magnetic equivalent circuits", *Mechatronics*, vol. 32, pp. 22–33, 2015. DOI: 10.1016/j.mechatronics.2015.10.007
The content of this post-print version is identical to the published paper but without the publisher's final layout or copy editing.

$$\left(\frac{\partial\mathcal{L}}{\partial\mathbf{u}_{tg}}\right)^T = \lambda p\left(\frac{\partial\mathbf{G}_t}{\partial\varphi}\mathbf{u}_{tg} + [\mathbf{0},\mathbf{0},\mathbf{I}]\,\bar{\mathbf{D}}\frac{\partial\mathbf{G}_c}{\partial\varphi}\bar{\mathbf{D}}^T\begin{bmatrix}\mathbf{H}_1^I\mathbf{i}_c^I\\ \mathbf{u}_{tm}\\ \mathbf{u}_{tg}\end{bmatrix}\right) + \left(\mathbf{G}_t + \mathbf{D}_g\mathbf{G}_c\mathbf{D}_g^T\right)\boldsymbol{\mu}$$
$$+\frac{1}{2}\lambda p\left(\mathbf{u}_{tg}^T\frac{\partial^2\mathbf{G}_t}{\partial\varphi\partial\mathbf{u}_{tg}}\mathbf{u}_{tg} + \left[(\mathbf{H}_1^I\mathbf{i}_c^I)^T,\mathbf{u}_{tm}^T,\mathbf{u}_{tg}^T\right]\bar{\mathbf{D}}\frac{\partial^2\mathbf{G}_c}{\partial\varphi\partial\mathbf{u}_{tg}}\bar{\mathbf{D}}^T\begin{bmatrix}\mathbf{H}_1^I\mathbf{i}_c^I\\ \mathbf{u}_{tm}\\ \mathbf{u}_{tg}\end{bmatrix}\right) \tag{8}$$
$$+\left(\left[\mathbf{D}_g\frac{\partial\mathbf{G}_c}{\partial\mathbf{u}_{tg}}\bar{\mathbf{D}}_c^T\mathbf{H}_1^I,\ \frac{\partial\mathbf{G}_t}{\partial\mathbf{u}_{tg}} + \mathbf{D}_g\frac{\partial\mathbf{G}_c}{\partial\mathbf{u}_{tg}}\mathbf{D}_g^T\right]\begin{bmatrix}\mathbf{i}_c^I\\ \mathbf{u}_{tg}\end{bmatrix} + \mathbf{D}_g\frac{\partial\mathbf{G}_c}{\partial\mathbf{u}_{tg}}\mathbf{D}_m^T\mathbf{u}_{tm}\right)^T\boldsymbol{\mu}$$

is indispensable for a practical implementation. For this purpose, two assumptions are made, which have proven to be practically feasible: First, the partial derivatives of $\mathbf{G}_t$ and $\mathbf{G}_c$ with respect to $\mathbf{i}_c^I$ and $\mathbf{u}_{tg}$ are neglected in (7) and (8). This significantly simplifies the complexity of the set of nonlinear equations to be solved. Second, it is assumed that a good initial guess of the solution at sampling interval k is given by the solution of the previous sampling interval $k-1$. This assumption is obviously valid if the angle φ and the desired torque τ^* do not significantly change from one step to the next. The angle φ is of course sufficiently smooth due to physics and the desired torque τ^* is defined in sufficiently smooth manner, i.e. step-like desired torques are not considered.

If these prerequisites are met, then the set of nonlinear equations

$$\begin{bmatrix}\left(\frac{\partial\mathcal{L}}{\partial\mathbf{i}_c^I}\right)^T\\ \left(\frac{\partial\mathcal{L}}{\partial\mathbf{u}_{tg}}\right)^T\\ \left(\frac{\partial\mathcal{L}}{\partial\lambda}\right)^T\\ \left(\frac{\partial\mathcal{L}}{\partial\boldsymbol{\mu}}\right)^T\end{bmatrix} = \begin{bmatrix}\mathbf{f}_{nl,1}\\ \mathbf{f}_{nl,2}\\ f_{nl,3}\\ \mathbf{f}_{nl,4}\end{bmatrix} = \mathbf{f}_{nl}\left(\mathbf{x}\right) = \mathbf{0}, \tag{9}$$

with the vector of unknowns $\mathbf{x}^T = \left[\left(\mathbf{i}_c^I\right)^T,\left(\mathbf{u}_{tg}\right)^T,\lambda,\boldsymbol{\mu}^T\right]$, can be solved by applying Newton iteration in the form[1]

$$\mathbf{x}_k^{j+1} = \mathbf{x}_k^j - \mathbf{J}_{nl}^{-1}(\mathbf{x}_k^j)\mathbf{f}_{nl}(\mathbf{x}_k^j), \quad \text{for } j = 0,\ldots,n_i-1, \tag{10}$$

with the initial condition $\mathbf{x}_k^0 = \mathbf{x}_{k-1}^{n_i}$ and the number of iterations n_i per sampling interval. The Jacobian $\mathbf{J}_{nl}$ of $\mathbf{f}_{nl}$ can be calculated analytically from (5), (7) and (8). Here again, neglecting the derivatives of the permeance matrices with respect to $\mathbf{u}_{tg}$ and $\mathbf{i}_c^I$ is meaningful and significantly simplifies the calculation. The entries of $\mathbf{J}_{nl}$ are summarized in Appendix A.

Summarizing, the proposed approach allows to calculate optimal coil currents $\mathbf{i}_c^*$ for a given desired torque τ^* in real-time for a magnetically nonlinear, non-fundamental wave PSM based on a magnetic equivalent circuit model. Before proceeding with the calculation of the real control inputs, i.e. the voltages $\mathbf{v}_c$, two simplifications frequently used in literature are analyzed from an optimal torque control point of view. First, magnetic saturation is neglected which yields a magnetically linear model. Still the non-sinusoidal flux characteristics is present. Afterwards, by assuming only fundamental wave components, the optimal torque control problem is discussed for the well-known dq0-model yielding the well-known results from literature.

3.2. Optimal currents: Magnetically linear case

If the iron is not saturated, then the permeance matrices $\mathbf{G}_t$ and $\mathbf{G}_c$ are independent of the mmfs and (1b) is a set of linear equations which can be solved analytically for $\boldsymbol{\psi}_c^I$ as a function of $\mathbf{i}_c^I$ by utilizing the matrix inversion lemma

$$\boldsymbol{\psi}_c^I = \left(\bar{\mathbf{D}}_c^I\right)^T\bar{\mathbf{D}}_c\mathbf{T}_l(\varphi)\left(\bar{\mathbf{D}}_c^T\mathbf{H}_1^I\mathbf{i}_c^I + \mathbf{D}_m^T\mathbf{u}_{tm}\right), \tag{11}$$

with

$$\mathbf{T}_l(\varphi) = \left(\mathbf{G}_c^{-1} + \mathbf{D}_g^T\mathbf{G}_t^{-1}\mathbf{D}_g\right)^{-1}. \tag{12}$$

Using (11) and (12) in (1a), the transformed coil currents $\mathbf{i}_c^I$ are given by

$$\mathbf{L}_c^I\frac{\mathrm{d}}{\mathrm{d}t}\mathbf{i}_c^I = -\frac{\partial\boldsymbol{\psi}_c^I}{\partial\varphi}\omega - R_c\mathbf{i}_c^I + \left(\bar{\mathbf{D}}_c^I\right)^T\mathbf{v}_c, \tag{13}$$

with the inductance matrix $\mathbf{L}_c^I$

$$\mathbf{L}_c^I(\varphi) = \left(\bar{\mathbf{D}}_c^I\right)^T\bar{\mathbf{D}}_c\mathbf{T}_l(\varphi)\bar{\mathbf{D}}_c^T\mathbf{H}_1^I, \tag{14}$$

which is, as was expected, non-singular. Furthermore, the partial derivative of the flux linkages with respect to φ can be written as

$$\frac{\partial\boldsymbol{\psi}_c^I}{\partial\varphi} = \left(\bar{\mathbf{D}}_c^I\right)^T\bar{\mathbf{D}}_c\frac{\partial\mathbf{T}_l}{\partial\varphi}\left(\bar{\mathbf{D}}_c^T\mathbf{H}_1^I\mathbf{i}_c^I + \mathbf{D}_m^T\mathbf{u}_{tm}\right). \tag{15}$$

The mathematical model in the magnetically linear case is completed by the torque equation

$$\tau = \frac{1}{2}p\left[\left(\mathbf{H}_1^I\mathbf{i}_c^I\right)^T,\mathbf{u}_{tm}^T\right]\begin{bmatrix}\bar{\mathbf{D}}_c\\ \mathbf{D}_m\end{bmatrix}\frac{\partial\mathbf{T}_l}{\partial\varphi}\left[\bar{\mathbf{D}}_c^T,\mathbf{D}_m^T\right]\begin{bmatrix}\mathbf{H}_1^I\mathbf{i}_c^I\\ \mathbf{u}_{tm}\end{bmatrix}. \tag{16}$$

[1] Of course, the Jacobian $\mathbf{J}_{nl}$ if $\mathbf{f}_{nl}$ is not inverted in (10) but the corresponding set of linear equations is solved for $\mathbf{x}_k^{j+1}$. For this purpose, efficient solvers for linear equations are used.

Post-print version of the article: W. Kemmetmüller, D. Faustner, and A. Kugi, “Optimal torque control of permanent magnet synchronous machines using magnetic equivalent circuits”, *Mechatronics*, vol. 32, pp. 22–33, 2015. DOI: 10.1016/j.mechatronics.2015.10.007
The content of this post-print version is identical to the published paper but without the publisher’s final layout or copy editing.

Based on this mathematical model for the magnetically linear case, the optimal independent coil currents can be found by solving the optimization problem

$$\min_{\mathbf{i}_c^I} \frac{1}{2} \left(\mathbf{i}_c^I\right)^T \mathbf{Q} \mathbf{i}_c^I \tag{17}$$

subject to the (nonlinear) scalar equality constraint

$$g = \tau\left(\mathbf{i}_c^I\right) - \tau^*. \tag{18}$$

Introducing the Lagrange function $\mathcal{L} = 1/2(\mathbf{i}_c^I)^T \mathbf{Q} \mathbf{i}_c^I + \lambda g$, the first order necessary optimality conditions take the form

$$\left(\frac{\partial \mathcal{L}}{\partial \mathbf{i}_c^I}\right)^T = \mathbf{Q}\mathbf{i}_c^I + \lambda p (\mathbf{H}_1^I)^T \bar{\mathbf{D}}_c \frac{\partial \mathbf{T}_l}{\partial \varphi} \left[\bar{\mathbf{D}}_c^T, \mathbf{D}_m^T\right] \begin{bmatrix} \mathbf{H}_1^I \mathbf{i}_c^I \\ \mathbf{u}_{tm} \end{bmatrix} \tag{19a}$$

$$\left(\frac{\partial \mathcal{L}}{\partial \lambda}\right)^T = \tau - \tau^*, \tag{19b}$$

which still constitutes a set of nonlinear equations. Thus, again Newton iteration is employed, as proposed in (10) for the general magnetically nonlinear case. The elements of the Jacobian $\mathbf{J}_l$ of (19) read as

$$J_{l,11} = \mathbf{Q} + \lambda p \left(\mathbf{H}_1^I\right)^T \bar{\mathbf{D}}_c \frac{\partial \mathbf{T}_l}{\partial \varphi} \bar{\mathbf{D}}_c^T \mathbf{H}_1^I \tag{20a}$$

$$J_{l,12} = J_{l,21}^T = p \left(\mathbf{H}_1^I\right)^T \bar{\mathbf{D}}_c \frac{\partial \mathbf{T}_l}{\partial \varphi} \left[\bar{\mathbf{D}}_c^T, \mathbf{D}_m^T\right] \begin{bmatrix} \mathbf{H}_1^I \mathbf{i}_c^I \\ \mathbf{u}_{tm} \end{bmatrix} \tag{20b}$$

$$J_{l,22} = \mathbf{0}. \tag{20c}$$

Thus, the method for the calculation of the optimal currents $\mathbf{i}_c^{I*}$ for a given desired torque τ^* in the magnetically linear case is similar to the magnetically nonlinear case but significantly less complex.

3.3. Optimal currents: Fundamental wave case

The inductance matrix $\mathbf{L}_c^I$ and $\mathbf{T}_l$ in (14) and (12) depend on the angle φ. If only fundamental wave components, i.e. components multiplied by $\sin(p\varphi)$ or $\cos(p\varphi)$, are considered, then the well-known dq0-transformation (Blondel Park transformation, see, e.g., [1, 2]) can be applied using the transformation matrix $\mathbf{T}_{dq}$

$$\mathbf{T}_{dq}(\varphi) = \begin{bmatrix} \cos(p\varphi) & \cos(p\varphi - \frac{2\pi}{3}) & \cos(p\varphi - \frac{4\pi}{3}) \\ \sin(p\varphi) & \sin(p\varphi - \frac{2\pi}{3}) & \sin(p\varphi - \frac{4\pi}{3}) \\ \frac{1}{2} & \frac{1}{2} & \frac{1}{2} \end{bmatrix}. \tag{21}$$

The resulting transformed magnetically linear fundamental wave model is given by, see also [1, 2, 38]

$$\frac{\mathrm{d}}{\mathrm{d}t} i_d = \frac{2}{3}\frac{1}{L_m}\left(-\frac{3}{2}L_m p\omega i_q - R_c i_d + v_d\right) \tag{22a}$$

$$\frac{\mathrm{d}}{\mathrm{d}t} i_q = \frac{2}{3}\frac{1}{L_m}\left(\frac{3}{2}L_m p\omega i_d - \frac{3}{2}\hat{J}\omega - R_c i_q + v_q\right), \tag{22b}$$

with the transformed currents and voltages

$$\begin{bmatrix} i_d \\ i_q \\ i_0 \end{bmatrix} = \mathbf{T}_{dq} \begin{bmatrix} i_{c1} \\ i_{c2} \\ i_{c3} \end{bmatrix}, \quad \begin{bmatrix} v_d \\ v_q \\ v_0 \end{bmatrix} = \mathbf{T}_{dq} \begin{bmatrix} v_{c1} \\ v_{c2} \\ v_{c3} \end{bmatrix} \tag{23}$$

and the inductance L_m. Since the electrical interconnection forces $v_0 = 0$, the zero component i_0 also vanishes, i.e. $i_0 = 0$. The corresponding transformed torque reads as, cf. [1, 2, 38]

$$\tau = 2p\hat{M}u_{ms}N_c i_q. \tag{24}$$

The constant coefficients L_m, $\hat{J}$ and $\hat{M}$ can be obtained from the magnetically linear model (11)-(16), e.g., by applying a Fourier analysis, see, also [38]. The determination of optimal currents for a given desired torque τ^* is trivial, since (24) implies $i_q^* = \tau^*/(2p\hat{M}u_{ms}N_c)$ and minimal losses are obtained by setting $i_d^* = 0$.

3.4. Simulation results

In this section, the optimal currents are evaluated based on the magnetically nonlinear model presented in [38], which was calibrated and validated by measurement results on a test stand. Basically, two major points should be discussed: What is the improvement by using the magnetically nonlinear or the magnetically linear model in comparison to the fundamental wave model typically used in literature? How does the number of Newton iterations n_i used in (10) influence the accuracy of the optimal solution?

As already shortly discussed in Section 3.1, besides the number of iterations n_i, the quality of the initial guess $\mathbf{x}_k^0$ used in the Newton iteration has an important influence on the accuracy. Obviously, it can be expected that the quality of the initial guess increases if the solution of the nonlinear equations – (9) for the magnetically nonlinear case and (19) for the magnetically linear case – only slightly changes from one sampling time $(k-1)T_s$ to the next kT_s. Clearly, the solution of the nonlinear equations changes due to changes in the rotor position φ and the desired torque τ^*. For the subsequent discussions, it is assumed that the desired torque τ^* is chosen constant. Additionally assuming a constant angular speed $\omega = \dot{\varphi}$, $\Delta\varphi = \varphi_k - \varphi_{k-1} = \omega T_s$ holds. The largest value of $\Delta\varphi$ arises at maximum speed ω_{max}, which is given by $\omega_{max} = 2\,\pi 20\,\mathrm{rad\,s^{-1}}$ (1200 rpm). In the subsequent simulation results, an angular speed of 830 rpm is chosen, which corresponds to a typical operating point of 70% of the maximum speed. Using a sampling time $T_s = 100\,\mu\mathrm{s}$, this results in $\Delta\varphi = 0.5°$.

Fig. 2 shows the results of the optimal currents obtained from the magnetically nonlinear model for different values of the desired torque τ^* from 0 N m to 3 N m, which corresponds to the maximum torque of the motor. In the left column, the three coil currents i_{c1}, i_{c2} and i_{c3} are depicted, which result from (10) with (9) for $n_i = 2$ iterations. The right column shows the resulting errors $\tau - \tau^*$

Post-print version of the article: W. Kemmetmüller, D. Faustner, and A. Kugi, "Optimal torque control of permanent magnet synchronous machines using magnetic equivalent circuits", *Mechatronics*, vol. 32, pp. 22–33, 2015. DOI: 10.1016/j.mechatronics.2015.10.007
The content of this post-print version is identical to the published paper but without the publisher's final layout or copy editing.

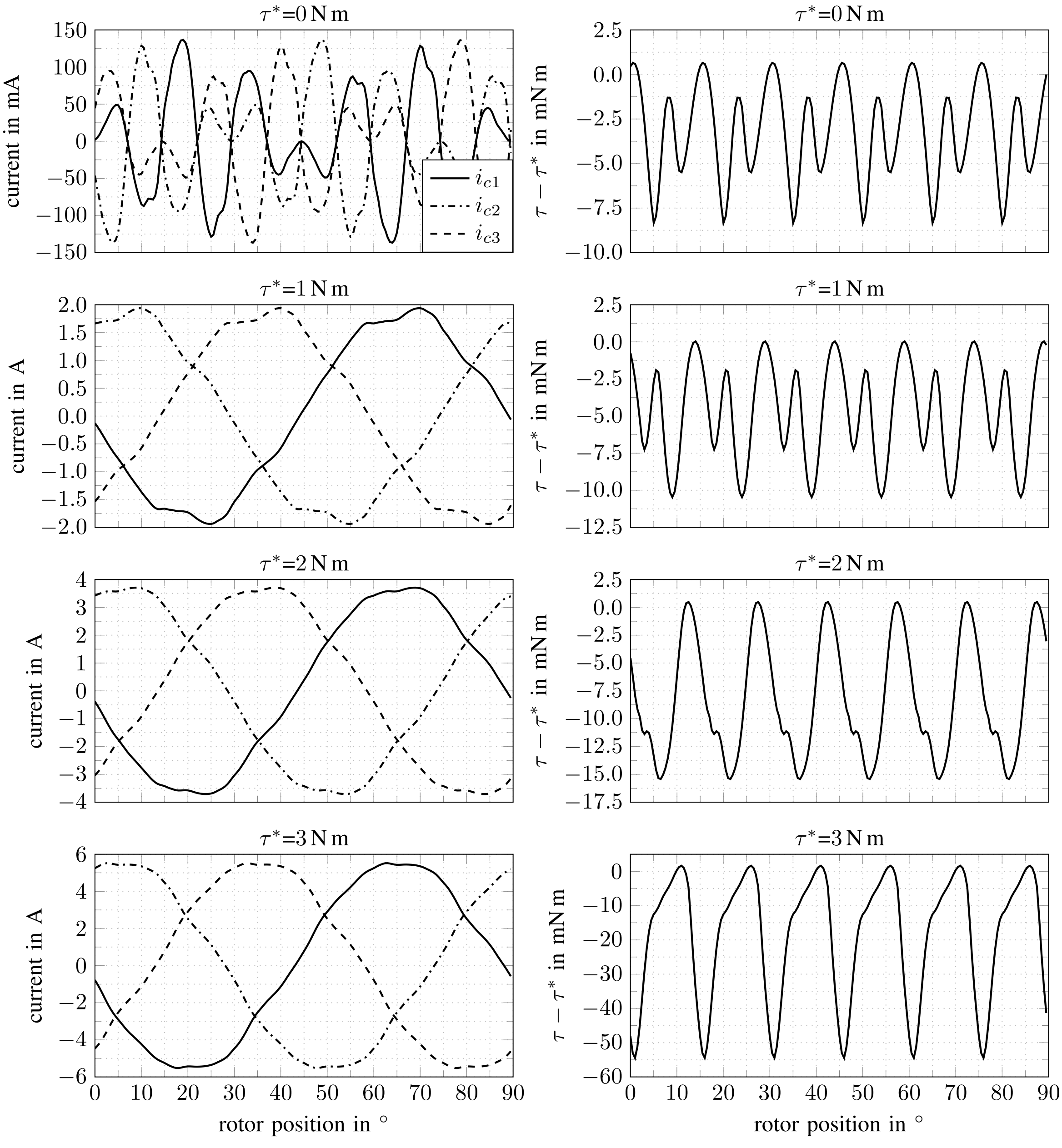

Figure 2: Optimal currents and torque error $\tau - \tau^*$ for the magnetically nonlinear case for different desired torques τ^*.

Post-print version of the article: W. Kemmetmüller, D. Faustner, and A. Kugi, "Optimal torque control of permanent magnet synchronous machines using magnetic equivalent circuits", *Mechatronics*, vol. 32, pp. 22–33, 2015. DOI: 10.1016/j.mechatronics.2015.10.007
The content of this post-print version is identical to the published paper but without the publisher's final layout or copy editing.

in the torque. It can be seen that the proposed method to calculate the optimal currents for the magnetically nonlinear model results in very small errors in the torque over the entire operating range of the motor. Taking a closer look at the optimal currents also reveals that the motor under consideration shows a significant nonlinear behavior due to magnetic saturation and non-fundamental wave characteristics of the coil fluxes. Especially, the case $\tau^* = 0\,\mathrm{N\,m}$ emphasizes the need to actively control the currents in order to suppress the pronounced cogging torque of the motor.

Since the calculation of the optimal currents given in Fig. 2 is based on the same magnetically nonlinear model which was used for the simulations, the torque errors given in Fig. 2 result solely from the non-exact solution of the constrained optimization problem (4), (5). Although two Newton iterations already yield a good accuracy in the torque, in Fig. 3 the influence of the number of iterations n_i on the accuracy of the torque is examined in more detail. As expected, a higher number of iterations improves the accuracy. For $n_i = 20$ almost perfect tracking of the desired torque is achieved. For the practical application, however, a compromise between accuracy and computation time must be found. As it will be shown in the measurement results discussed later on, a number of $n_i = 2$ iterations turns out to be a good choice. Since the magnetically linear case is numerically less expensive, a higher number of iterations could be used. However, the errors resulting from the numeric solution of the optimization problem are very small already after 2 iterations such that $n_i = 2$ is also a good choice for the magnetically linear case.

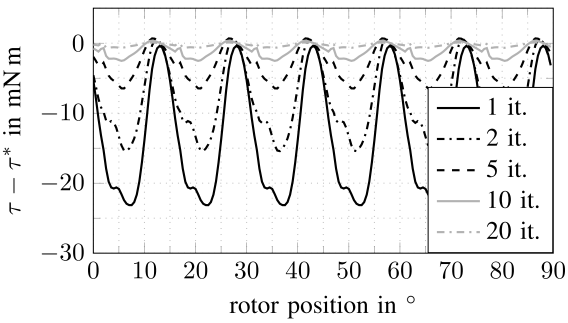

Figure 3: Influence of the number of Newton iterations on the accuracy of the optimal solution for the magnetically nonlinear case for $\tau^* = 2\,\mathrm{N\,m}$.

Finally, the results given in Fig. 4 show the advantages gained from the usage of the magnetically nonlinear model for the calculation of optimal coil currents. Taking a look at the case $\tau^* = 0\,\mathrm{N\,m}$ first, it turns out that the optimal currents obtained from the magnetically nonlinear and the magnetically linear model exhibit a similar behavior. Even though the results of the magnetically nonlinear model show better torque accuracy, the results of the magnetically linear model are still comparably good. This is due to the fact that for the resulting small values of the currents the influence of the magnetic saturation of the core is negligible. The results based on the fundamental wave model (dq0-model), however, are significantly worse. As a matter of fact, it is not possible to systematically include the cogging torque in the dq0-model, which results in $i_{c1} = i_{c2} = i_{c3} = 0$ as the optimal values. Then, the resulting torque τ is equal to the cogging torque of the motor. The advantages of using the magnetically nonlinear model instead of the magnetically linear model can be recognized for large values of τ^*. The results for $\tau^* = 2\,\mathrm{N\,m}$ in Fig. 4 show that neglecting magnetic saturation entails an error in the torque of approximately $150\,\mathrm{mN\,m}$.

In conclusion, these first simulation results demonstrate that considering the magnetic nonlinearities in the calculation of the optimal currents yields a significant improvement of the accuracy of the torque in comparison to methods based on a magnetically linear model or the dq0-model.

4. Flatness-based current control

In the previous section, optimal values of the currents $\mathbf{i}_c^I$ have been calculated such that the torque τ tracks a desired torque τ^* and the copper losses are minimized. These results are the basis for a flatness-based feedforward and feedback control strategy to be developed in this section.

4.1. Magnetically nonlinear case

The solution of the optimization problem (4), (5) results in optimal currents $\mathbf{i}_c^{I*}$ and optimal values $\mathbf{u}_{tg}^*$ of the mmfs of the tree permeances. Considering (1b) with (2), the corresponding optimal values of the flux linkages $\boldsymbol{\psi}_c^{I*}$ are given by

$$\boldsymbol{\psi}_c^{I*} = \left(\bar{\mathbf{D}}_c^I\right)^T \bar{\mathbf{D}}_c \mathbf{G}_c \left(\bar{\mathbf{D}}_c^T \mathbf{H}_1^I \mathbf{i}_c^{I*} + \mathbf{D}_g^T \mathbf{u}_{tg}^* + \mathbf{D}_m^T \mathbf{u}_{tm}\right). \tag{25}$$

Using this result in (1a), i.e. in

$$\frac{\mathrm{d}}{\mathrm{d}t}\boldsymbol{\psi}_c^{I*} = -R_c \mathbf{i}_c^{I*} + \left(\bar{\mathbf{D}}_c^I\right)^T \mathbf{v}_c^*, \tag{26}$$

with $(\bar{\mathbf{D}}_c^\perp)^T \mathbf{v}_c^* = \mathbf{0}$, yields the feedforward part $\mathbf{v}_c^*$ of the control input $\mathbf{v}_c$ in the form

$$\mathbf{v}_c^* = \mathbf{H}_1^I \left(\frac{\mathrm{d}}{\mathrm{d}t}\boldsymbol{\psi}_c^{I*} + R_c \mathbf{i}_c^{I*}\right). \tag{27}$$

The time derivative of the optimal coil flux linkage $\boldsymbol{\psi}_c^{I*}$ can be calculated from (25)

$$\frac{\mathrm{d}}{\mathrm{d}t}\boldsymbol{\psi}_c^{I*} = \left(\bar{\mathbf{D}}_c^I\right)^T \bar{\mathbf{D}}_c \mathbf{G}_c \left(\bar{\mathbf{D}}_c^T \mathbf{H}_1^I \frac{\mathrm{d}}{\mathrm{d}t}\mathbf{i}_c^{I*} + \mathbf{D}_g^T \frac{\mathrm{d}}{\mathrm{d}t}\mathbf{u}_{tg}^*\right) + \left(\bar{\mathbf{D}}_c^I\right)^T \bar{\mathbf{D}}_c \frac{\partial \mathbf{G}_c}{\partial \varphi} \left(\bar{\mathbf{D}}_c^T \mathbf{H}_1^I \mathbf{i}_c^{I*} + \mathbf{D}_g^T \mathbf{u}_{tg}^* + \mathbf{D}_m^T \mathbf{u}_{tm}\right)\omega, \tag{28}$$

Post-print version of the article: W. Kemmetmüller, D. Faustner, and A. Kugi, “Optimal torque control of permanent magnet synchronous machines using magnetic equivalent circuits”, *Mechatronics*, vol. 32, pp. 22–33, 2015. DOI: 10.1016/j.mechatronics.2015.10.007
The content of this post-print version is identical to the published paper but without the publisher’s final layout or copy editing.

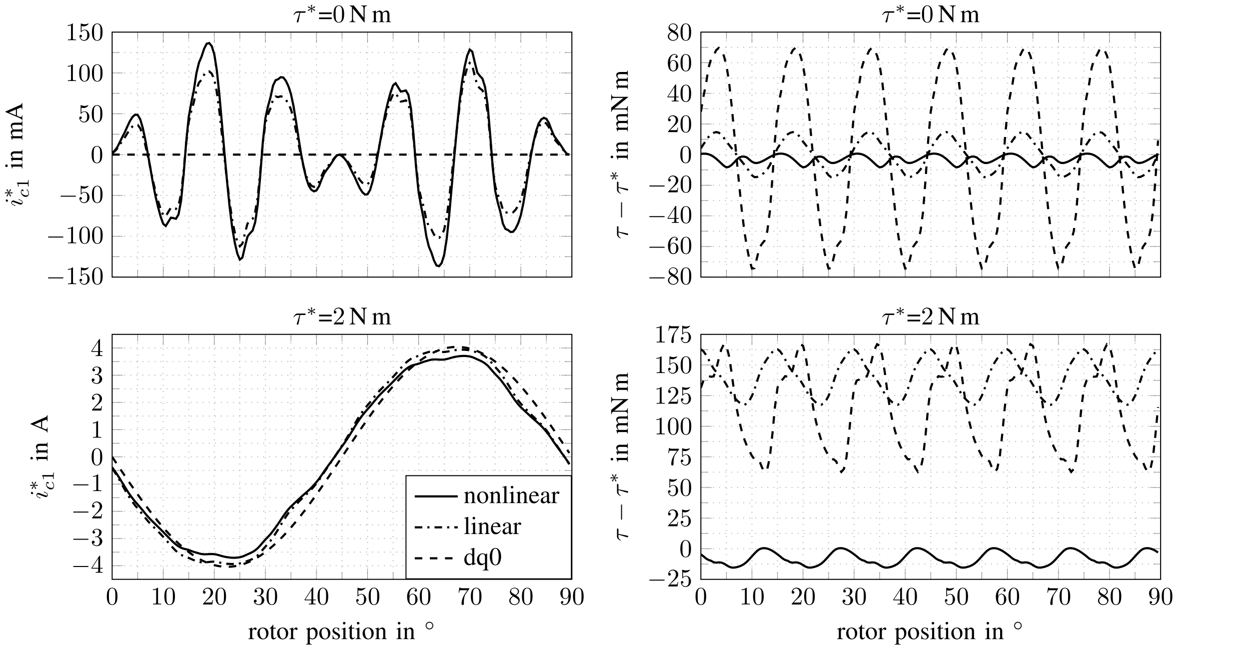

Figure 4: Optimal current i_{c1}^* and torque error $\tau - \tau^*$ for the magnetically nonlinear, the magnetically linear and the fundamental wave case for different desired torques τ^*.

where again the partial derivatives of $\mathbf{G}_c$ with respect to $\mathbf{i}_c^I$ and $\mathbf{u}_{tg}$ have been neglected. To obtain the time derivatives of the optimal current $\mathbf{i}_c^{I*}$ and the optimal mmfs of the tree permeances $\mathbf{u}_{tg}^*$, the first order optimality conditions (9) are utilized. The total time derivative of $\mathbf{f}_{nl}$ reads as

$$\frac{\mathrm{d}}{\mathrm{d}t}\mathbf{f}_{nl} = \mathbf{J}_{nl}\frac{\mathrm{d}}{\mathrm{d}t}\begin{bmatrix}\mathbf{i}_c^{I*}\\ \mathbf{u}_{tg}^*\\ \lambda^*\\ \boldsymbol{\mu}^*\end{bmatrix} + \frac{\partial \mathbf{f}_{nl}}{\partial \varphi}\omega + \frac{\partial \mathbf{f}_{nl}}{\partial \tau^*}\frac{\mathrm{d}}{\mathrm{d}t}\tau^* = \mathbf{0}, \qquad (29)$$

with the Jacobian $\mathbf{J}_{nl}$ and the partial derivatives $\partial\mathbf{f}_{nl}/\partial\varphi$ and $\partial\mathbf{f}_{nl}/\partial\tau^*$ summarized in Appendix A. The time derivatives can be easily obtained from this set of linear equations, since $\mathbf{J}_{nl}$ is non-singular.

Remark 1. *The calculation of* $\mathrm{d}\boldsymbol{\psi}_c^{I*}/\mathrm{d}t$ *as described in* (28) *and* (29) *is computationally expensive, even if the Jacobian* $\mathbf{J}_{nl}$ *needed in* (29) *has already been calculated in the Newton iteration* (10)*. Given the fact that the control strategy is implemented using a fixed sampling time* T_s*, the approximation*

$$\frac{\mathrm{d}}{\mathrm{d}t}\boldsymbol{\psi}_c^{I*}(kT_s) \approx \frac{\boldsymbol{\psi}_{c,k}^{I*} - \boldsymbol{\psi}_{c,k-1}^{I*}}{T_s} \qquad (30)$$

can be obtained. Using this approximation in (27) *significantly simplifies the calculation of the feedforward control part and is therefore preferable for the practical application. The errors resulting from this approximation are typically small due to the small sampling time* T_s*.*

With (27) an optimal feedforward control law $\mathbf{v}_c^*$ is given. To cope with model inaccuracies and external disturbances, in addition a feedback controller has to be designed. In a practical application, measurement of the coil flux linkage is not reasonable. Thus, a control strategy based on the measured coil currents has to be developed.

Using the feedforward control (27) in (1a), the following differential equation for the error in the coil flux linkage can be formulated

$$\frac{\mathrm{d}}{\mathrm{d}t}\left(\boldsymbol{\psi}_c^I - \boldsymbol{\psi}_c^{I*}\right) = -R_c\mathbf{e}_i^I + \left(\bar{\mathbf{D}}_c^I\right)^T\mathbf{v}_c^c, \qquad (31)$$

with the current error $\mathbf{e}_i^I = \mathbf{i}_c^I - \mathbf{i}_c^{I*}$ and the feedback part $\mathbf{v}_c^c$ of the input voltage $\mathbf{v}_c = \mathbf{v}_c^c + \mathbf{v}_c^*$. The coil flux linkage error can be found as a function of the current error $\mathbf{e}_i^I$ and the error $\mathbf{e}_u$ in the mmfs of the tree permeances, $\mathbf{e}_u = \mathbf{u}_{tg} - \mathbf{u}_{tg}^*$, from the following set of equations

$$\begin{aligned}\begin{bmatrix}\mathbf{I}\\ \mathbf{0}\end{bmatrix}\left(\boldsymbol{\psi}_c^I - \boldsymbol{\psi}_c^{I*}\right) = &\begin{bmatrix}\left(\bar{\mathbf{D}}_c^I\right)^T\bar{\mathbf{D}}_c\mathbf{G}_c\bar{\mathbf{D}}_c^T\mathbf{H}_1^I\\ \mathbf{D}_g\mathbf{G}_c\bar{\mathbf{D}}_c^T\mathbf{H}_1^I\end{bmatrix}\mathbf{e}_i^I\\ &+\begin{bmatrix}\left(\bar{\mathbf{D}}_c^I\right)^T\bar{\mathbf{D}}_c\mathbf{G}_c\mathbf{D}_g^T\\ \mathbf{G}_t + \mathbf{D}_g\mathbf{G}_c\mathbf{D}_g^T\end{bmatrix}\mathbf{e}_u.\end{aligned} \qquad (32)$$

This equation results from (1b) assuming[2] $\mathbf{G}_c(-\bar{\mathbf{D}}^T\bar{\mathbf{u}}_t,\varphi) \approx \mathbf{G}_c(-\bar{\mathbf{D}}^T\bar{\mathbf{u}}_t^*,\varphi)$ and $\mathbf{G}_t(\mathbf{u}_{tg},\varphi) \approx \mathbf{G}_t(\mathbf{u}_{tg}^*,\varphi)$. The solution of (32) for the coil flux linkage error reads as

$$\psi_c^I - \psi_c^{I*} = \left(\bar{\mathbf{D}}_c^I\right)^T\bar{\mathbf{D}}_c\mathbf{T}_l\bar{\mathbf{D}}_c^T\mathbf{H}_1^I\mathbf{e}_i^I = \mathbf{L}_c^I\left(\bar{\mathbf{u}}_t^*,\varphi\right)\mathbf{e}_i^I, \qquad (33)$$

[2] Note that this assumption is basically equal to assuming that the control errors are small.

Post-print version of the article: W. Kemmetmüller, D. Faustner, and A. Kugi, "Optimal torque control of permanent magnet synchronous machines using magnetic equivalent circuits", *Mechatronics*, vol. 32, pp. 22–33, 2015. DOI: 10.1016/j.mechatronics.2015.10.007
The content of this post-print version is identical to the published paper but without the publisher's final layout or copy editing.

with $\mathbf{T}_l$ from (12). Please note that, in contrast to the magnetically linear case, the inductance matrix $\mathbf{L}_c^I$ is both a function of $\bar{\mathbf{u}}_t^*$ and φ in the magnetically nonlinear case. Using (33) in (31), the error dynamics is given by

$$\mathbf{L}_c^I \frac{\mathrm{d}}{\mathrm{d}t}\mathbf{e}_i^I = -\left(\bar{\mathbf{D}}_c^I\right)^T \bar{\mathbf{D}}_c \left(\frac{\partial \mathbf{T}_l}{\partial \varphi}\omega + \frac{\partial \mathbf{T}_l}{\partial \bar{\mathbf{u}}_t^*}\frac{\mathrm{d}\bar{\mathbf{u}}_t^*}{\mathrm{d}t}\right)\bar{\mathbf{D}}_c^T \mathbf{H}_1^I \mathbf{e}_i^I - R_c \mathbf{e}_i^I + \left(\bar{\mathbf{D}}_c^I\right)^T \mathbf{v}_c^c. \tag{34}$$

The feedback control law $\mathbf{v}_c^c$

$$\mathbf{v}_c^c = \mathbf{H}_1^I \left[\left(\bar{\mathbf{D}}_c^I\right)^T \bar{\mathbf{D}}_c \left(\frac{\partial \mathbf{T}_l}{\partial \varphi}\omega + \frac{\partial \mathbf{T}_l}{\partial \bar{\mathbf{u}}_t^*}\frac{\mathrm{d}\bar{\mathbf{u}}_t^*}{\mathrm{d}t}\right)\bar{\mathbf{D}}_c^T \mathbf{H}_1^I + R_c\right]\mathbf{e}_i^I + \mathbf{H}_1^I \mathbf{L}_c^I \left(-\lambda_{1i}\mathbf{e}_i^I - \lambda_{0i}\int_0^t \mathbf{e}_i^I \mathrm{d}t\right), \tag{35}$$

with $\lambda_{1i}, \lambda_{0i} > 0$, finally yields an exponentially stable current error dynamics.

Remark 2. *The feedback control law* (35) *again includes some parts which are computationally expensive. However, in a practical implementation, neglecting the first part on the right hand side of* (35) *turns out to be a feasible simplification if the current error* $\mathbf{e}_i^I$ *is small. Then, the simplified feedback control law reads as*

$$\mathbf{v}_c^c = \mathbf{H}_1^I \mathbf{L}_c^I \left(-\lambda_{1i}\mathbf{e}_i^I - \lambda_{0i}\int_0^t \mathbf{e}_i^I \mathrm{d}t\right). \tag{36}$$

The inductance matrix $\mathbf{L}_c^I$ *is, in the magnetically nonlinear case, both a function of* φ *and* $\bar{\mathbf{u}}_t^*$. *Thus, it reflects the changes due to the rotor position* φ *and saturation of the iron. Fig. 5(a) shows the entries* $L_{c,kj}^I$, $k,j = 1,2$ *of* $\mathbf{L}_c^I$ *for* $\tau_d^* = 0\,\mathrm{N\,m}$ *of the motor under consideration. It can be seen that the inductances show a significant variation with respect to a change in the rotor position. A comparison of the self inductance* $L_{c,11}^I$ *for* $\tau_d^* = 0\,\mathrm{N\,m}$ *with* $L_{c,11}^I$ *for* $\tau_d^* = 3\,\mathrm{N\,m}$ *in Fig. 5(b) reveals that the influence of saturation on the inductance matrix* $\mathbf{L}_c^I$ *is rather small and can therefore be neglected in a practical application, i.e.* $\mathbf{L}_c^I(\bar{\mathbf{u}}_t^*, \varphi) \approx \mathbf{L}_c^I(\bar{\mathbf{u}}_t^0, \varphi)$ *using a nominal operating point* $\bar{\mathbf{u}}_t^0$. *As will be discussed in Section 5 a further simplification using the average value* $\bar{\mathbf{L}}_c^I$,

$$\bar{\mathbf{L}}_c^I = \frac{2}{\pi}\int_0^{\frac{\pi}{2}} \mathbf{L}_c^I(\bar{\mathbf{u}}_t^0, \varphi)\mathrm{d}\varphi, \tag{37}$$

does not significantly deteriorate the current control accuracy for the considered motor. Of course, it is required to check if the above prerequisites are fulfilled for a specific motor before these simplifications can be made.

4.2. Magnetically linear case

The calculation of the feedforward control $\mathbf{v}_c^*$ is significantly simplified for the magnetically linear case. Given

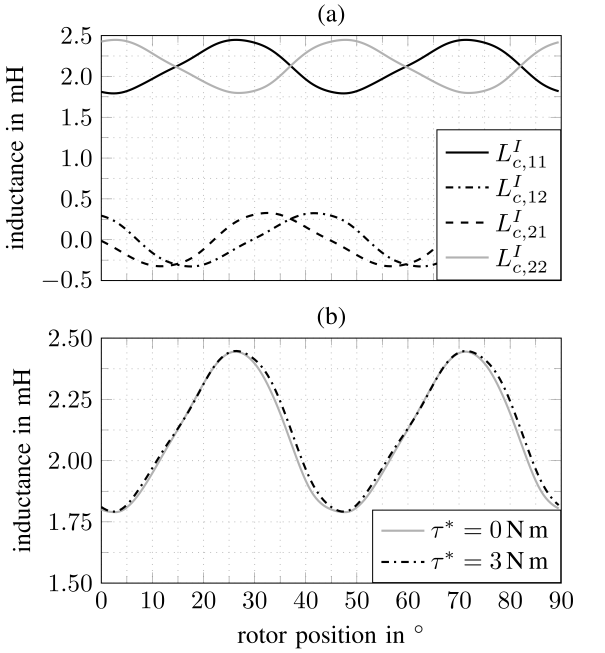

Figure 5: (a) Entries of the inductance matrix $\mathbf{L}_c^I$ for $\tau^* = 0\,\mathrm{N\,m}$. (b) Comparison of $L_{c,11}^I$ for $\tau^* = 0\,\mathrm{N\,m}$ and $\tau^* = 3\,\mathrm{N\,m}$.

the optimal values $\mathbf{i}_c^{I*}$ of the coil currents, the corresponding voltage can be obtained from (13) in the form

$$\mathbf{v}_c^* = \mathbf{H}_1^I \left(\mathbf{L}_c^I \frac{\mathrm{d}}{\mathrm{d}t}\mathbf{i}_c^{I*} + \frac{\partial \boldsymbol{\psi}_c^{I*}}{\partial \varphi}\omega + R_c \mathbf{i}_c^{I*}\right), \tag{38}$$

with $\partial \boldsymbol{\psi}_c^{I*}/\partial \varphi$ resulting from using the optimal currents $\mathbf{i}_c^{I*}$ in (15). The time derivative of $\mathbf{i}_c^{I*}$ in (38) can be obtained as a solution of

$$\frac{\mathrm{d}\mathbf{f}_l}{\mathrm{d}t} = \mathbf{J}_l \frac{\mathrm{d}}{\mathrm{d}t}\begin{bmatrix}\mathbf{i}_c^{I*}\\ \lambda^*\end{bmatrix} + \frac{\partial \mathbf{f}_l}{\partial \varphi}\omega + \frac{\partial \mathbf{f}_l}{\partial \tau^*}\frac{\mathrm{d}}{\mathrm{d}t}\tau^* = \mathbf{0}, \tag{39}$$

using $\mathbf{f}_l$, being the right-hand side of (19), and $\mathbf{J}_l$ from (20). The partial derivatives of $\mathbf{f}_l$ with respect to φ are given by

$$\frac{\partial \mathbf{f}_{l,1}}{\partial \varphi} = \lambda p \left(\mathbf{H}_1^I\right)^T \bar{\mathbf{D}}_c \frac{\partial^2 \mathbf{T}_l}{\partial \varphi^2}\begin{bmatrix}\bar{\mathbf{D}}_c^T \mathbf{H}_1^I \mathbf{i}_c^I\\ \mathbf{D}_m^T \mathbf{u}_{tm}\end{bmatrix} \tag{40a}$$

$$\frac{\partial f_{l,2}}{\partial \varphi} = \frac{1}{2}p\left[\left(\mathbf{H}_1^I \mathbf{i}_c^I\right)^T, \mathbf{u}_{tm}^T\right]\begin{bmatrix}\bar{\mathbf{D}}_c\\ \mathbf{D}_m\end{bmatrix}\frac{\partial^2 \mathbf{T}_l}{\partial \varphi^2}\left[\bar{\mathbf{D}}_c^T, \mathbf{D}_m^T\right]\begin{bmatrix}\mathbf{H}_1^I \mathbf{i}_c^I\\ \mathbf{u}_{tm}\end{bmatrix} \tag{40b}$$

and $\partial \mathbf{f}_{l,1}/\partial \tau^* = \mathbf{0}$, $\partial f_{l,2}/\partial \tau^* = -1$ holds. For the practical implementation, it again proves to be useful to approximate $\mathrm{d}\mathbf{i}_c^{I*}/\mathrm{d}t$ by

$$\frac{\mathrm{d}\mathbf{i}_c^{I*}}{\mathrm{d}t}(kT_s) \approx \frac{\mathbf{i}_{c,k}^{I*} - \mathbf{i}_{c,k-1}^{I*}}{T_s}, \tag{41}$$

cf. Remark 1.

The dynamics of the current error $\mathbf{e}_i^I = \mathbf{i}_c^I - \mathbf{i}_c^{I*}$ is given by

$$\mathbf{L}_c^I \frac{\mathrm{d}}{\mathrm{d}t}\mathbf{e}_i^I = -\left(\bar{\mathbf{D}}_c^I\right)^T \bar{\mathbf{D}}_c \frac{\partial \mathbf{T}_l}{\partial \varphi} \bar{\mathbf{D}}_c^T \mathbf{H}_1^I \mathbf{e}_i^I \omega - R_c \mathbf{e}_i^I + \left(\bar{\mathbf{D}}_c^I\right)^T \mathbf{v}_c^c \tag{42}$$

and the feedback control law $\mathbf{v}_c^c$

$$\begin{aligned}\mathbf{v}_c^c =& \mathbf{H}_1^I \left(\left(\bar{\mathbf{D}}_c^I\right)^T \bar{\mathbf{D}}_c \frac{\partial \mathbf{T}_l}{\partial \varphi} \bar{\mathbf{D}}_c^T \mathbf{H}_1^I \mathbf{e}_i^I \omega + R_c \mathbf{e}_i^I \right) \\ &+ \mathbf{H}_1^I \left(-\lambda_{1i} \mathbf{e}_i^I - \lambda_{0i} \int_0^t \mathbf{e}_i^I \mathrm{d}t \right),\end{aligned} \tag{43}$$

with $\lambda_{0i}, \lambda_{1i} > 0$, renders the error dynamics exponentially stable. As discussed in Remark 2 for the magnetically nonlinear case, also in the magnetically linear case the first part of the right hand side of (43) can be neglected and $\mathbf{L}_c^I(\varphi)$ can be approximated by the average $\bar{\mathbf{L}}_c^I$ for the considered motor without introducing significant errors.

4.3. Fundamental wave case

For the fundamental wave model, again a flatness-based control strategy in the form of $v_d = v_d^* + v_d^c$ and $v_q = v_q^* + v_q^c$ is developed. In this case, the feedforward part is simply given by

$$v_d^* = \frac{3}{2} L_m p \omega i_q^* \tag{44a}$$

$$v_q^* = R_c i_q^* + \frac{3}{2} \hat{J} \omega + \frac{3}{2} L_m \frac{\mathrm{d}}{\mathrm{d}t} i_q^*, \tag{44b}$$

where $i_d^* = 0$ and $i_q^* = 2\tau^*/(p\hat{M})$ are used. It can be easily seen that the feedback control law

$$v_d^c = R_c e_{id} + \frac{3}{2} L_m p \omega e_{iq} + \frac{3}{2} L_m \left(-\lambda_{1i} e_{id} - \lambda_{0i} \int_0^t e_{id} \mathrm{d}t \right) \tag{45a}$$

$$v_q^c = R_c e_{iq} - \frac{3}{2} L_m p \omega e_{id} + \frac{3}{2} L_m \left(-\lambda_{1i} e_{iq} - \lambda_{0i} \int_0^t e_{iq} \mathrm{d}t \right), \tag{45b}$$

in combination with the feedforward control (44) yields an exponentially stable dynamics for the errors $e_{id} = i_d - i_d^*$ and $e_{iq} = i_q - i_q^*$ with $\lambda_{0i}, \lambda_{1i} > 0$. A simplified version of (45) in the form

$$v_d^c = \frac{3}{2} L_m \left(-\lambda_{1i} e_{id} - \lambda_{0i} \int_0^t e_{id} \mathrm{d}t \right) \tag{46a}$$

$$v_q^c = \frac{3}{2} L_m \left(-\lambda_{1i} e_{iq} - \lambda_{0i} \int_0^t e_{iq} \mathrm{d}t \right), \tag{46b}$$

which is frequently used in practical applications, only yields a small reduction of the control accuracy.

5. Measurement results

To compare and to evaluate the performance of the proposed torque control concepts, measurement results on the test stand depicted in Fig. 6 are presented. The test stand comprises the PSM under consideration which is coupled to a harmonic drive (load motor) via a torque sensor and a high resolution encoder. By means of the harmonic drive it is possible to fix the angular speed of the motor at a desired value. The torque generated by the PSM is measured by the torque sensor. The PSM is controlled by a three-phase bridge using MOSFETs as power switches. A fixed pulse-width modulation frequency of 10 kHz is used and the duty cycles of the individual half-bridges are utilized to adjust the voltages v_{ck}, $k = 1, 2, 3$, applied to the coils. The control strategies described in the Sections 3 and 4 were implemented on a dSPACE 1103 real-time hardware equipped with a 1 GHz PowerPC processor. The fundamental wave control strategy was implemented at a sampling time of 100 µs, while for the magnetically linear and the magnetically nonlinear control strategy an increased sampling time of 200 µs had to be used due to the higher numerical complexity. Moreover, average values $\bar{\mathbf{L}}_c^I$ of the inductance matrix according to (37) and $n_i = 2$ Newton iterations have been used. For the subsequent measurements, a fixed angular speed of 4 rpm was chosen. Please note that this slow speed prevents excitation of resonances of the mechanical setup which would deteriorate the accuracy of the measured torque. In the next section, it will be proven that the proposed control concept also works well for fast angular speeds.

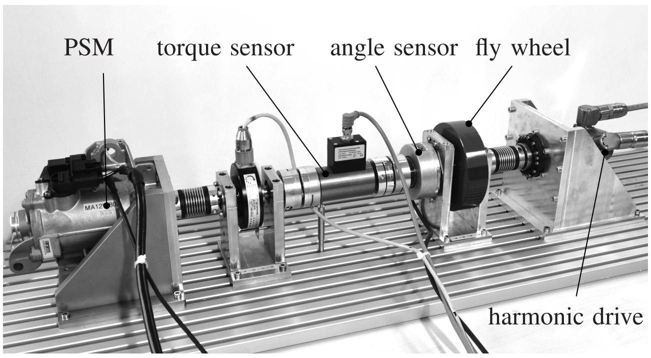

Figure 6: Setup of the test stand.

Fig. 7 shows the measurement results of the coil current i_{c1} and the torque τ for the three control strategies of Sections 3 and 4, and for $\tau^* = 0, 1$ and 2 N m. In accordance with the simulation results in Fig. 4, the fundamental wave model performs worst, especially for $\tau^* = 0$ N m. This is, as has been already discussed, due to the fact that the cogging torque is not included in the fundamental wave model. The magnetically linear and the magnetically nonlinear control strategies, however, show almost identical behavior for $\tau^* = 0$ N m. The benefits of the nonlinear

Post-print version of the article: W. Kemmetmüller, D. Faustner, and A. Kugi, "Optimal torque control of permanent magnet synchronous machines using magnetic equivalent circuits", *Mechatronics*, vol. 32, pp. 22–33, 2015. DOI: 10.1016/j.mechatronics.2015.10.007

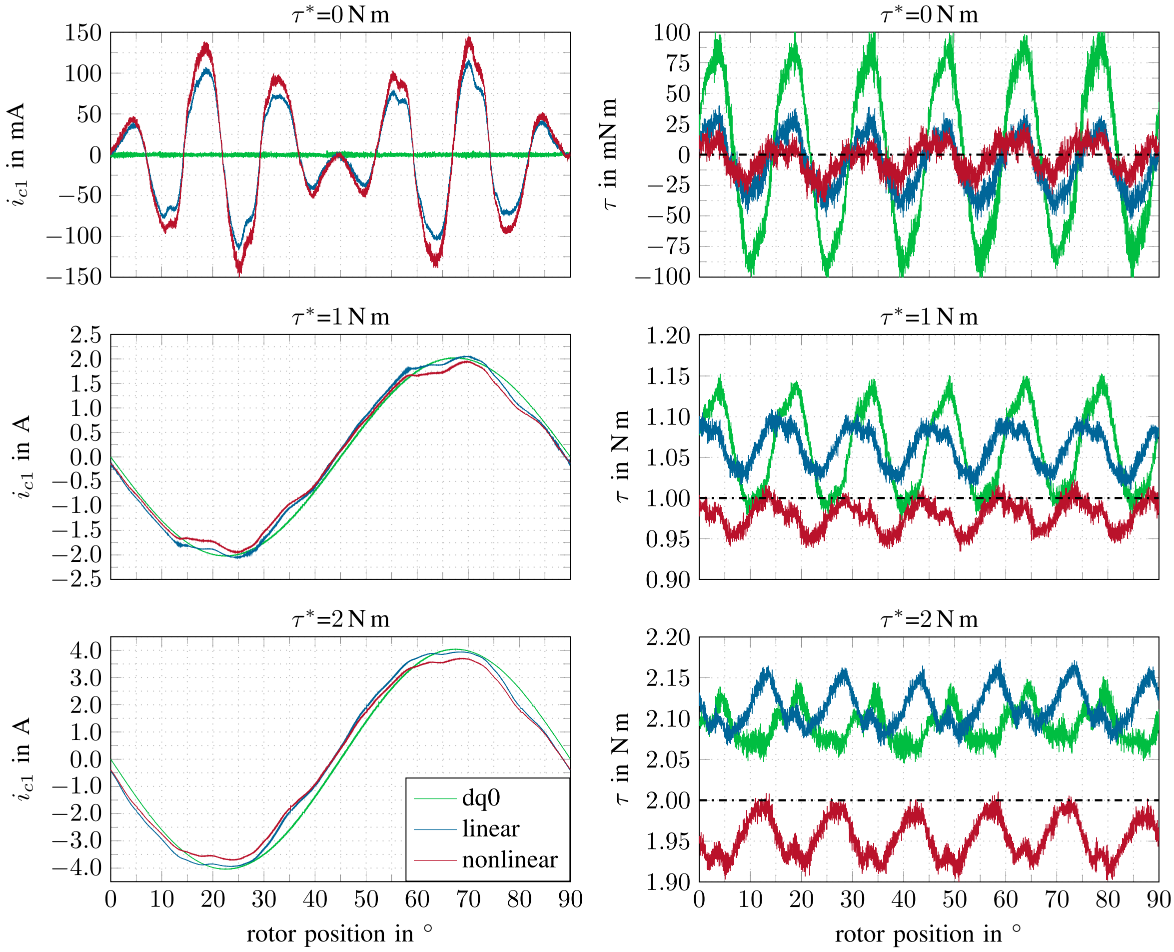

Figure 7: Comparison of the measured coil current i_{c1} and torque τ of the fundamental wave (dq0), the magnetically linear and the magnetically nonlinear control strategy for $\tau^* = 0, 1$ and $2\,\mathrm{N\,m}$.

control strategy in comparison to the linear and the fundamental wave strategy is evident for increased desired torques $\tau^* = 1\,\mathrm{N\,m}$ and $\tau^* = 2\,\mathrm{N\,m}$, see Fig. 7.

In Fig. 8 the corresponding control input v_{c1} and the current control error $i_{c1} - i_{c1}^*$ for the nonlinear control strategy for $\tau^* = 2\,\mathrm{N\,m}$ are depicted. Taking a closer look at the control input, characteristic steps can be seen in the measurements. These steps result from the compensation of the nonlinearities of the three phase bridge in the vicinity of zero currents. The measurement of the current control error shows that the current is controlled to the desired value within the measurement accuracy, which is in the order of $\pm 7\,\mathrm{mA}$ in the present experimental setup.

It has to be mentioned that in comparison to the simulation results an increased deviation from the desired torque values is present in the measurements. This can be attributed to two facts:

1. The mechanical setup, in particular the flexible couplings, introduces small periodic disturbances which are also measured by the torque sensor.
2. The model, as a matter of fact, does not perfectly represent the real system behavior, see also [38]. These model errors are then reflected in the measured torque.

It is worth mentioning that the measurements of the torque sensor are only used to evaluate the control quality but are, of course, not part of the feedback loop. Thus, even if the current perfectly tracks the desired current, cf. Fig. 8, the errors in the model from current to torque are still present. However, it is well documented that the proposed nonlinear control concept which is based on the magentic equivalent circuit model of [38] brings along a significant improvement of the torque control accuracy. In conclusion, the measurement results show that the proposed nonlinear control concept is practically feasible and yields good tracking results of the desired torque.

6. Control of angular speed

There are a number of applications where the PSM is used in a torque-controlled mode as e.g. in electrical power steering systems or traction applications. Therein, it is evident that an improvement of the torque control

Post-print version of the article: W. Kemmetmüller, D. Faustner, and A. Kugi, "Optimal torque control of permanent magnet synchronous machines using magnetic equivalent circuits", *Mechatronics*, vol. 32, pp. 22–33, 2015. doi: 10.1016/j.mechatronics.2015.10.007

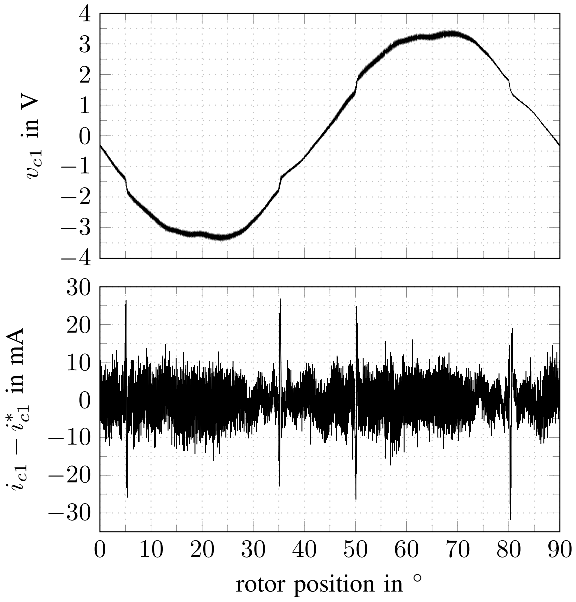

Figure 8: Control input v_{c1} and current control error $i_{c1} - i_{c1}^*$ of the nonlinear control strategy for $\tau^* = 2\,\mathrm{N\,m}$.

accuracy directly yields an improved system performance. In most cases, however, the torque (or current) controller is used as a subordinate control loop for an outer speed or position control. In this section, it will be outlined that the improved accuracy of the proposed nonlinear torque control strategy also entails an improvement of a cascaded speed control loop.

To do so, the test stand depicted in Fig. 6 is adapted by removing the torque sensor and the harmonic drive, directly coupling the fly wheel and the angle sensor to the PSM. The angular speed $\omega = \dot{\varphi}$ of the resulting system can be described in the form

$$\frac{\mathrm{d}}{\mathrm{d}t}\omega = \frac{1}{\theta_m}\left(-d_v\omega - d_c \tanh\left(\frac{\omega}{\omega_0}\right) + \tau\right), \tag{47}$$

with the moment of inertia θ_m of the PSM including the fly wheel and the viscous damping coefficient d_v. The Coulomb friction of the setup is approximated by the term $d_c \tanh(\omega/\omega_0)$, where ω_0 is used to parameterize the steepness at $\omega = 0$.

In a cascaded controller design it is usually assumed that the torque controller is very fast and thus the error between the desired torque τ^* and the real torque τ generated by the PSM is negligible. Setting $\tau = \tau^*$ in (47), τ can be considered as a virtual control input to the system. A two degrees-of-freedom flatness-based control concept of the form $\tau^* = \tau^{**} + \tau^{*c}$ is frequently employed for the speed control of such a system in literature. The feedforward part τ^{**} and the feedback part τ^{*c} are given by

$$\tau^{**} = d_v\omega^* + d_c \tanh\left(\frac{\omega^*}{\omega_0}\right) + \theta_m \frac{\mathrm{d}}{\mathrm{d}t}\dot{\omega}^* \tag{48a}$$

$$\tau^{*c} = \theta_m\left(-\lambda_{1\omega}e_\omega - \lambda_{0\omega}\int_0^t e_\omega \mathrm{d}t\right), \tag{48b}$$

with the at least twice continuously differentiable desired angular speed ω^*, the controller parameters $\lambda_{1\omega}, \lambda_{0\omega} > 0$ and the speed error $e_\omega = \omega - \omega^*$.

Remark 3. *For the control strategies developed in Sections 3 and 4, the time derivative of the desired torque τ^* is necessary, cf.* (29) *for the magnetically nonlinear case,* (39) *for the magnetically linear case and* (44) *for the fundamental wave case. The controller part τ^{*c} includes the measured speed ω, which can cause problems when performing this differentiation. Thus, for the practical application it is often useful to set $\dot{\tau}^* \approx \dot{\tau}^{**}$, with τ^{**} from* (48a)*. A similar idea can of course also be used for the simplified derivations given by* (30) *and* (41)*.*

Fig. 9 presents the measurement results of the speed controller for constant desired speed ω^*. Therein, the speed controller (48) was used with the three torque control strategies of Sections 3 and 4 in the subordinate control loop. It can be seen that for the fast angular speed of 200 rpm only small differences between the three torque control strategies are visible, while for slow angular speeds the magnetically nonlinear and the magnetically linear control strategies yield significantly better results compared to the fundamental wave case. The main reason for the errors in the speed are the errors in the subordinate torque control, where the frequency of the resulting disturbance is proportional to the angular speed. The high frequency disturbances for 200 rpm are well suppressed by the mechanical inertia, while for lower angular speed an increased influence can be seen. Only small differences can be seen between the magnetically linear and the magnetically nonlinear case since the average torque necessary to drive the mechanical setup is rather small. As depicted in Fig. 7, the magnetically linear and magnetically nonlinear control strategies show similar performance in this torque range. This result proves that the proposed torque control strategy is beneficial also for speed control, in particular for slow angular speeds as they typically occur for precision position tasks in robotics.

Remark 4. *A number of papers dealing with the speed and the position control of PSMs with pronounced cogging torque (as the PSM under consideration) has been reported in literature, see, e.g., [46–49]. A frequent approach to tackle this problem is to consider the torque ripple in the form of a (periodic) disturbance for the speed controller, which is compensated by more or less involved control strategies. In comparison to these approaches, using a torque controller as presented in Sections 3 and 4 already ensures that only small torque ripples are produced*

Post-print version of the article: W. Kemmetmüller, D. Faustner, and A. Kugi, “Optimal torque control of permanent magnet synchronous machines using magnetic equivalent circuits”, *Mechatronics*, vol. 32, pp. 22–33, 2015. DOI: 10.1016/j.mechatronics.2015.10.007

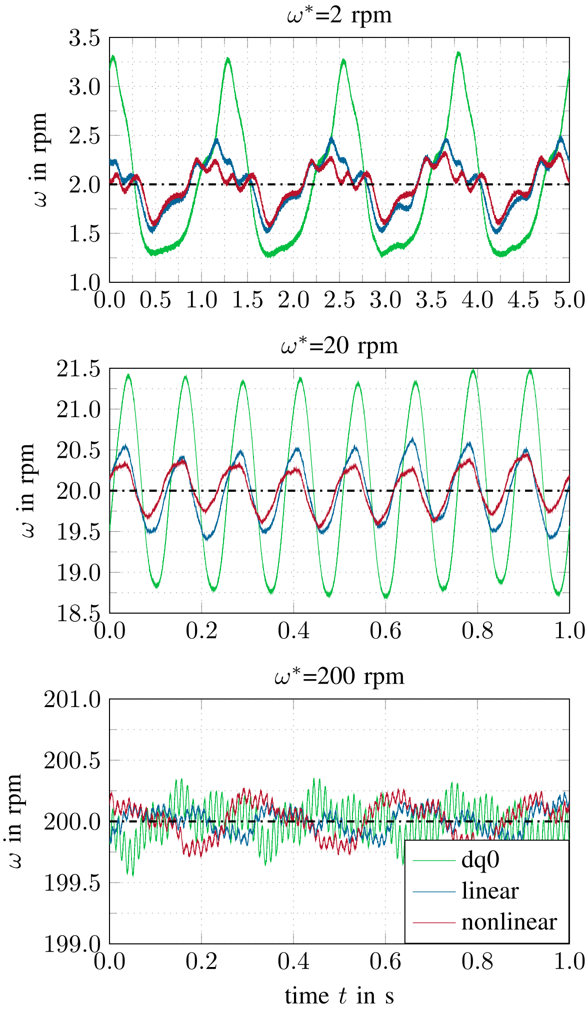

Figure 9: Comparison of the speed control for constant desired speed using the torque control strategies of Sections 3 and 4.

by the PSM. Thus, the accurate control of the speed is significantly simplified. Especially for drive trains with small inertia or low angular stiffness, this approach can be considered advantageous.

To analyze the current control accuracy, the desired and the measured coil current i_{c1}^* and i_{c1}, respectively, are presented in Fig. 10. The corresponding control input, i.e. the coil voltage v_{c1}, is also depicted there. It can be seen that, although the current has to track a rather complex desired current, a very good tracking accuracy can be achieved.

Finally, in Fig. 11 the results of an experiment, which drives the PSM to its operational limits, are given. Here, the desired speed is changed from -600 rpm to 600 rpm (half of the rated speed) within 0.6 s using approx. 2.5-times the rated torque of the PSM. An almost perfect tracking accuracy of the desired speed is obtained using the speed control strategy from (48) and the magnetically nonlinear torque control strategy of Section 4.1. The corresponding coil current i_{c1} and coil voltage v_{c1} are also depicted in Fig. 11.

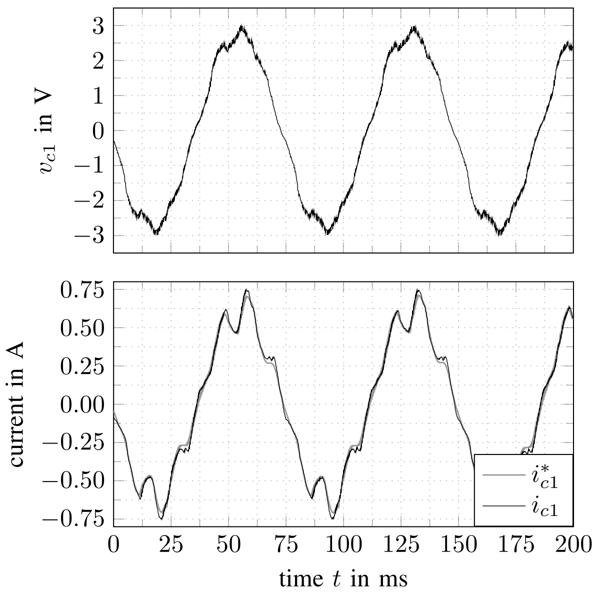

Figure 10: Control input v_{c1} and current control accuracy for $\omega^* =$ 200 rpm.

In conclusion, the experiments performed in this section and in Section 3.4 prove the practical feasibility and demonstrate the improvements in control accuracy compared to classical control strategies based on a fundamental wave model.

7. Conclusion

In this work, an optimal torque control for PSMs described by MEC models was presented and tested on an experimental setup. It was shown that by systematically incorporating the magnetic saturation and the non-fundamental wave characteristics into the model and the controller design, significant improvement of the control accuracy and the performance can be obtained. Moreover, the practical feasibility was demonstrated by means of measurements on an experimental setup.

Up to now, limitation of the control input, i.e. the coil voltages, has not been taken into account. Thus, future research will be devoted to the question how to extend the proposed nonlinear control strategy to the field weakening range of the motor. Moreover, since the MEC modeling approach is not limited to PSMs, the application of this method to other motor designs as switched reluctance, synchronous reluctance or induction machines will be examined. Finally, the usage of the MEC model in a model predictive control setup is a further topic of current research.

Post-print version of the article: W. Kemmetmüller, D. Faustner, and A. Kugi, "Optimal torque control of permanent magnet synchronous machines using magnetic equivalent circuits", *Mechatronics*, vol. 32, pp. 22–33, 2015. DOI: 10.1016/j.mechatronics.2015.10.007
The content of this post-print version is identical to the published paper but without the publisher's final layout or copy editing.

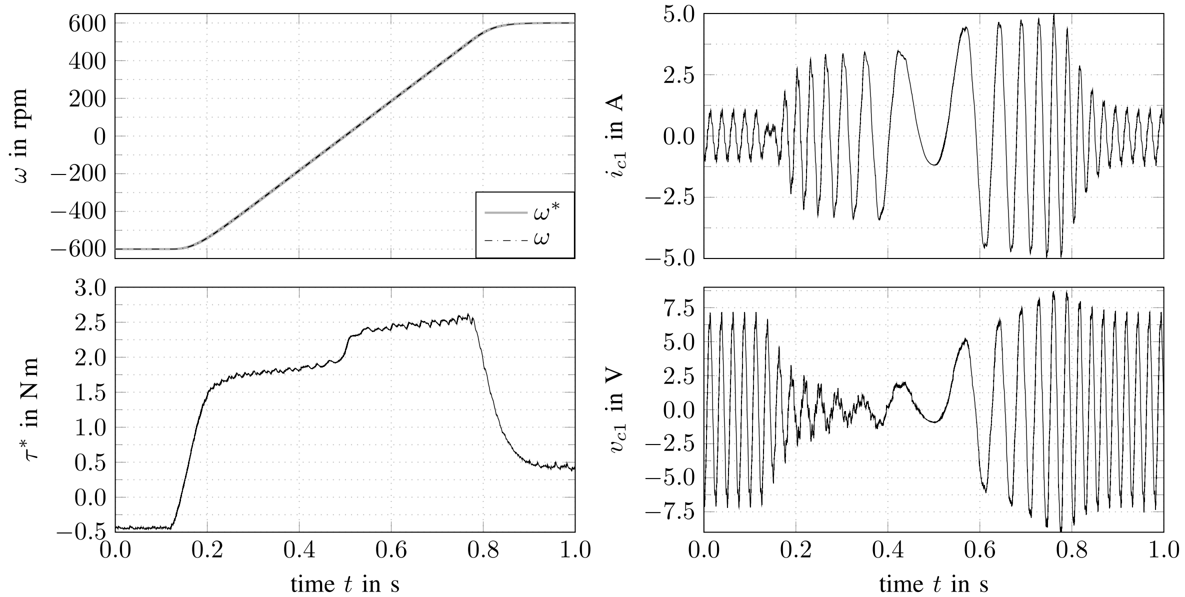

Figure 11: Change of desired speed using the speed controller of (48) and the magnetically nonlinear control strategy of Section 4.1.

Appendix A. Entries of the Jacobian $\mathbf{J}_{nl}$ of $\mathbf{f}_{nl}$

This appendix summarizes the entries of the Jacobian $\mathbf{J}_{nl}$ for the magnetically nonlinear case[3]. Given $(\mathbf{f}_{nl,1})^T = \partial\mathcal{L}/\partial\mathbf{i}_c^I$, the corresponding partial derivatives are given by

$$\frac{\partial \mathbf{f}_{nl,1}}{\partial \mathbf{i}_c^I} = \mathbf{Q} + \lambda p \left[(\mathbf{H}_1^I)^T, \mathbf{0}, \mathbf{0}\right] \bar{\mathbf{D}} \frac{\partial \mathbf{G}_c}{\partial \varphi} \bar{\mathbf{D}}^T \begin{bmatrix} \mathbf{H}_1^I \\ \mathbf{0} \\ \mathbf{0} \end{bmatrix} \tag{A.1a}$$

$$\frac{\partial \mathbf{f}_{nl,1}}{\partial \mathbf{u}_{tg}} = \lambda p \left[(\mathbf{H}_1^I)^T, \mathbf{0}, \mathbf{0}\right] \bar{\mathbf{D}} \frac{\partial \mathbf{G}_c}{\partial \varphi} \bar{\mathbf{D}}^T \begin{bmatrix} \mathbf{0} \\ \mathbf{0} \\ \mathbf{I} \end{bmatrix} \tag{A.1b}$$

$$\frac{\partial \mathbf{f}_{nl,1}}{\partial \lambda} = p \left[(\mathbf{H}_1^I)^T, \mathbf{0}, \mathbf{0}\right] \bar{\mathbf{D}} \frac{\partial \mathbf{G}_c}{\partial \varphi} \bar{\mathbf{D}}^T \begin{bmatrix} \mathbf{H}_1^I \mathbf{i}_c^I \\ \mathbf{u}_{tm} \\ \mathbf{u}_{tg} \end{bmatrix} \tag{A.1c}$$

$$\frac{\partial \mathbf{f}_{nl,1}}{\partial \boldsymbol{\mu}} = \left(\mathbf{H}_1^I\right)^T \bar{\mathbf{D}}_c \mathbf{G}_c \mathbf{D}_g^T \tag{A.1d}$$

The partial derivatives of $(\mathbf{f}_{nl,2})^T = \partial\mathcal{L}/\partial\mathbf{u}_{tg}$ result in

$$\frac{\partial \mathbf{f}_{nl,2}}{\partial \mathbf{u}_{tg}} = \lambda p \left(\frac{\partial \mathbf{G}_t}{\partial \varphi} + [\mathbf{0}, \mathbf{0}, \mathbf{I}] \bar{\mathbf{D}} \frac{\partial \mathbf{G}_c}{\partial \varphi} \bar{\mathbf{D}}^T \begin{bmatrix} \mathbf{0} \\ \mathbf{0} \\ \mathbf{I} \end{bmatrix} \right) \tag{A.2a}$$

$$\frac{\partial \mathbf{f}_{nl,2}}{\partial \lambda} = p \left(\frac{\partial \mathbf{G}_t}{\partial \varphi} \mathbf{u}_{tg} + [\mathbf{0}, \mathbf{0}, \mathbf{I}] \bar{\mathbf{D}} \frac{\partial \mathbf{G}_c}{\partial \varphi} \bar{\mathbf{D}}^T \begin{bmatrix} \mathbf{H}_1^I \mathbf{i}_c^I \\ \mathbf{u}_{tm} \\ \mathbf{u}_{tg} \end{bmatrix} \right) \tag{A.2b}$$

$$\frac{\partial \mathbf{f}_{nl,2}}{\partial \boldsymbol{\mu}} = \mathbf{G}_t + \mathbf{D}_g \mathbf{G}_c \mathbf{D}_g^T \tag{A.2c}$$

[3] Note that the derivatives of the permeance matrices $\mathbf{G}_t$ and $\mathbf{G}_c$ with respect to $\mathbf{u}_{tg}$ and $\mathbf{i}_c^I$ are assumed to be negligible.

and the partial derivatives of $(f_{nl,3})^T = \partial\mathcal{L}/\partial\lambda$ and $(\mathbf{f}_{nl,4})^T = \partial\mathcal{L}/\partial\boldsymbol{\mu}$ are given by

$$\frac{\partial f_{nl,3}}{\partial \lambda} = \mathbf{0} \tag{A.3a}$$

$$\frac{\partial \mathbf{f}_{nl,3}}{\partial \boldsymbol{\mu}} = \mathbf{0} \tag{A.3b}$$

$$\frac{\partial \mathbf{f}_{nl,4}}{\partial \boldsymbol{\mu}} = \mathbf{0}. \tag{A.3c}$$

The remaining entries of $\mathbf{J}_{nl}$ result from the symmetry of this matrix.

Post-print version of the article: W. Kemmetmüller, D. Faustner, and A. Kugi, "Optimal torque control of permanent magnet synchronous machines using magnetic equivalent circuits", *Mechatronics*, vol. 32, pp. 22–33, 2015. DOI: 10.1016/j.mechatronics.2015.10.007
The content of this post-print version is identical to the published paper but without the publisher's final layout or copy editing.

The partial derivatives of $\mathbf{f}_{nl}$ with respect to φ read as

$$\frac{\partial \mathbf{f}_{nl,1}}{\partial \varphi} = \lambda p \left[\left(\mathbf{H}_1^I\right)^T, \mathbf{0}, \mathbf{0} \right] \bar{\mathbf{D}} \frac{\partial^2 \mathbf{G}_c}{\partial \varphi^2} \bar{\mathbf{D}}^T \begin{bmatrix} \mathbf{H}_1^I \mathbf{i}_c^I \\ \mathbf{u}_{tm} \\ \mathbf{u}_{tg} \end{bmatrix} + \left(\mathbf{H}_1^I\right)^T \bar{\mathbf{D}}_c \frac{\partial \mathbf{G}_c}{\partial \varphi} \mathbf{D}_g^T \boldsymbol{\mu} \tag{A.4a}$$

$$\frac{\partial \mathbf{f}_{nl,2}}{\partial \varphi} = \lambda p \left(\frac{\partial^2 \mathbf{G}_t}{\partial \varphi^2} \mathbf{u}_{tg} + [\mathbf{0}, \mathbf{0}, \mathbf{I}] \bar{\mathbf{D}} \frac{\partial^2 \mathbf{G}_c}{\partial \varphi^2} \bar{\mathbf{D}}^T \begin{bmatrix} \mathbf{H}_1^I \mathbf{i}_c^I \\ \mathbf{u}_{tm} \\ \mathbf{u}_{tg} \end{bmatrix} \right) + \left(\frac{\partial \mathbf{G}_t}{\partial \varphi} + \mathbf{D}_g \frac{\partial \mathbf{G}_c}{\partial \varphi} \mathbf{D}_g^T \right) \boldsymbol{\mu} \tag{A.4b}$$

$$\frac{\partial f_{nl,3}}{\partial \varphi} = \frac{1}{2} p \Big(\mathbf{u}_{tg}^T \frac{\partial^2 \mathbf{G}_t}{\partial \varphi^2} \mathbf{u}_{tg} + \left[(\mathbf{H}_1^I \mathbf{i}_c^I)^T, \mathbf{u}_{tm}^T, \mathbf{u}_{tg}^T \right] \bar{\mathbf{D}} \frac{\partial^2 \mathbf{G}_c}{\partial \varphi^2} \bar{\mathbf{D}}^T \begin{bmatrix} \mathbf{H}_1^I \mathbf{i}_c^I \\ \mathbf{u}_{tm} \\ \mathbf{u}_{tg} \end{bmatrix} \Big) \tag{A.4c}$$

$$\frac{\partial \mathbf{f}_{nl,4}}{\partial \varphi} = \left[\mathbf{D}_g \frac{\partial \mathbf{G}_c}{\partial \varphi} \bar{\mathbf{D}}_c^T \mathbf{H}_1^I, \frac{\partial \mathbf{G}_t}{\partial \varphi} + \mathbf{D}_g \frac{\partial \mathbf{G}_c}{\partial \varphi} \mathbf{D}_g^T \right] \begin{bmatrix} \mathbf{i}_c^I \\ \mathbf{u}_{tg} \end{bmatrix} + \mathbf{D}_g \frac{\partial \mathbf{G}_c}{\partial \varphi} \mathbf{D}_m^T \mathbf{u}_{tm} \tag{A.4d}$$

and $\partial \mathbf{f}_{nl,1}/\partial \tau^* = \mathbf{0}$, $\partial \mathbf{f}_{nl,2}/\partial \tau^* = \mathbf{0}$, $\partial \mathbf{f}_{nl,3}/\partial \tau^* = -1$ and $\partial \mathbf{f}_{nl,4}/\partial \tau^* = \mathbf{0}$.

References

[1] W. Leonhard, Control of Electrical Drives, Springer, 2001.

[2] P. C. Krause, O. Wasynczuk, S. D. Sudhoff, Analysis of Electric Machinery and Drive Systems, IEEE Press, 2002.

[3] C. Xia, Q. Geng, X. Gu, T. Shi, Z. Song, Input-output feedback linearization and speed control of a surface permanent-magnet synchronous wind generator with the boost-chopper converter, IEEE Trans. Ind. Electron. 59 (9) (2012) 3489–3500.

[4] S. Rebouh, A. Kaddouri, R. Abdessemed, A. Haddoun, Nonlinear control by input-output linearization scheme for ev permanent magnet synchronous motor, in: Proc. of the IEEE Vehicle Power and Propulsion Conference (VPPC), Arlington, TX, USA, 2007, pp. 185–190.

[5] J. Solsona, M. Valla, C. Muravchik, Nonlinear control of a permanent magnet synchronous motor with disturbance torque estimation, IEEE Trans. Energy Convers. 15 (2) (2000) 163–168.

[6] M. Morawiec, The adaptive backstepping control of permanent magnet synchronous motor supplied by current source inverter, IEEE Trans. Ind. Informat. 9 (2) (2013) 1047–1055.

[7] J. Zhou, Y. Wang, Real-time nonlinear adaptive backstepping speed control for a pm synchronous motor, Control Engineering Practice 13 (10) (2005) 1259–1269.

[8] M. Karabacak, H. Eskikurt, Speed and current regulation of a permanent magnet synchronous motor via nonlinear and adaptive backstepping control, Mathematical and Computer Modelling 53 (9–10) (2011) 2015–2030.

[9] M. Khanchoul, M. Hilairet, D. Normand-Cyrot, A passivity-based controller under low sampling for speed control of pmsm, Control Engineering Practice 26 (2014) 20–27.

[10] G. Tadmor, Control of a combined gto/igbt drive system for low torque ripple in a large permanent magnet synchronous motor, IEEE Trans. Control Syst. Technol. 12 (1) (2004) 21–35.

[11] P. Nicklasson, R. Ortega, G. Espinosa-Perez, C. Jacobi, Passivity-based control of a class of blondel-park transformable electric machines, IEEE Trans. Autom. Control 42 (5) (1997) 629–647.

[12] C. Lai, K. Shyu, A novel motor drive design for incremental motion system via sliding-mode control method, IEEE Trans. Ind. Electron. 52 (2) (2005) 499–507.

[13] X. Zhang, L. Sun, K. Zhao, L. Sun, Nonlinear speed control for pmsm system using sliding-mode control and disturbance compensation techniques, IEEE Trans. Power Electron. 28 (3) (2013) 1358–1365.

[14] I. Baik, K. Kim, M. Youn, Robust nonlinear speed control of pm synchronous motor using boundary layer integral sliding mode control technique, IEEE Trans. Control Syst. Technol. 8 (1) (2000) 47–54.

[15] S. Chai, L. Wang, E. Rogers, Model predictive control of a permanent magnet synchronous motor with experimental validation, Control Engineering Practice 21 (11) (2013) 1584–1593.

[16] M. Preindl, S. Bolognani, Model predictive direct speed control with finite control set of pmsm drive systems, IEEE Trans. Power Electron. 28 (2) (2013) 1007–1015.

[17] R. Errouissi, M. Ouhrouche, W. Chen, A.M.Trzynadlowski, Robust nonlinear predictive controller for permanent-magnet synchronous motors with an optimized cost function, IEEE Trans. Ind. Electron. 59 (7) (2012) 2849–2858.

[18] Y. Ren, Z. Zhu, J. Liu, Direct torque control of permanent-magnet synchronous machine drives with a simple duty ratio regulator, IEEE Trans. Ind. Electron. 61 (10) (2014) 5249–5258.

[19] C. Choi, J. Seok, R. Lorenz, Wide-speed direct torque and flux control for interior pm synchronous motors operating at voltage and current limits, IEEE Trans. Ind. Appl. 49 (1) (2013) 109–117.

[20] C. Ortega, A. Arias, C. Caruana, J. Balcells, G. Asher, Improved waveform quality in the direct torque control of matrix-converter-fed pmsm drives, IEEE Trans. Ind. Electron. 57 (6) (2010) 2101–2110.

[21] P. Mattavelli, L. Tubiana, M. Zigliotto, Torque-ripple reduction in pm synchronous motor drives using repetitive current control, IEEE Trans. Power Electron. 20 (6) (2005) 1423–1431.

[22] B. Grcar, P. Cafuta, G. Stumberger, A. Stankovic, Control-based reduction of pulsating torque for pmac machines, IEEE Trans. Energy Convers. 17 (2) (2002) 169–175.

[23] W. Qian, S. Panda, J. Xu, Speed ripple minimization in pm synchronous motor using iterative learning control, IEEE Trans. Energy Convers. 20 (1) (2005) 53–61.

[24] V. Petrovic, R. Ortega, A. Stankovic, G. Tadmor, Design and implementation of an adaptive controller for torque ripple minimization in pm synchronous motors, IEEE Trans. Power Electron. 15 (5) (2000) 871–880.

[25] Y. Mohamed, A hybrid-type variable-structure instantaneous torque control with a robust adaptive torque observer for a high-performance direct-drive pmsm, IEEE Trans. Ind. Electron. 54 (5) (2007) 2491–2499.

[26] J. Xu, S. Panda, Y. Pan, T. Lee, B. Lam, A modular control scheme for pmsm speed control with pulsating torque minimization, IEEE Trans. Ind. Electron. 51 (3) (2004) 526–536.

[27] D. Flieller, N. Nguyen, P. Wira, G. Sturtzer, D. Abdeslam, J. Merckle, A self-learning solution for torque ripple reduction for nonsinusoidal permanent-magnet motor drives based on artificial neural networks, IEEE Trans. Ind. Electron. 61 (2) (2014) 655–666.

[28] Y. Ait-Gougam, R. Ibtiouen, O. Touhami, J. Louis, M. Gabsi, Inverse modelling and pulsating torque minimization of salient pole non-sinusoidal synchronous machines, Electric Power Systems Research 78 (2008) 88–96.

[29] F. Aghili, Adaptive reshaping of excitation current for accurate torque control of brushless motors, IEEE Transactions on Control Systems Technology 16 (2) (2008) 356–364.

[30] D. Hanselman, Minimum torque ripple, maximum efficiency excitation of brushless permanent magnet motors, IEEE Trans. Ind. Electron. 41 (3) (1994) 292–300.

[31] G. Sturtzer, D. Flieller, J. Louis, Mathematical and experimental method to obtain the inverse modeling of nonsinusoidal and saturated synchronous reluctance motors, IEEE Trans. Energy Convers. 18 (4) (2003) 494–500.

Post-print version of the article: W. Kemmetmüller, D. Faustner, and A. Kugi, “Optimal torque control of permanent magnet synchronous machines using magnetic equivalent circuits”, *Mechatronics*, vol. 32, pp. 22–33, 2015. DOI: 10.1016/j.mechatronics.2015.10.007
The content of this post-print version is identical to the published paper but without the publisher’s final layout or copy editing.

[32] S. Jurkovic, E. Strangas, Design and analysis of a high-gain observer for the operation of spm machines under saturation, IEEE Trans. Energy Convers. 26 (2) (2011) 417–427.
[33] H. Seok-Hee, T. Jahns, W. Soong, A magnetic circuit model for an ipm synchronous machine incorporating moving airgap and cross-coupled saturation effects, in: Proc. of the IEEE International Electric Machines & Drives Conference, Antalya, Turkey, 2007, pp. 21–26.
[34] C. Mademlis, V. Agelidis, On considering magnetic saturation with maximum torque to current control in interior permanent magnet synchronous motor drives, IEEE Trans. Energy Convers. 16 (3) (2001) 246–252.
[35] S. Jung, J. Hong, K. Nam, Current minimizing torque control of the ipmsm using ferrari's method, IEEE Trans. Power Electron. 28 (12) (2013) 5603–5617.
[36] J. Lee, K. Nam, S. Choi, S. Kwon, Loss-minimizing control of pmsm with the use of polynomial approximations, IEEE Trans. Power Electron. 24 (4) (2009) 1071–1082.
[37] A. Consoli, G. Scarcella, G. Scelba, A. Testa, Steady-state and transient operation of ipmsms under maximum-torque-per-ampere control, IEEE Trans. Ind. Appl. 46 (1) (2010) 121–129.
[38] W. Kemmetmüller, D. Faustner, A. Kugi, Modeling of a permanent magnet synchronous machine with internal magnet using magnetic equivalent circuits, IEEE Trans. Magn. 50 (6) (2014) 8101314.
[39] D. Faustner, W. Kemmetmüller, A. Kugi, Magnetic equivalent circuit modeling of a saturated surface-mounted permanent magnet synchronous machine, in: Proc. of the 8th Vienna Int. Conference on Mathematical Modelling (MATHMOD), Vienna, Austria, 2015, pp. 360–365.
[40] D. Faustner, W. Kemmetmüller, A. Kugi, Flatness-based torque control of saturated surface-mounted permanent magnet synchronous machines, IEEE Trans. Control Syst. Technol. (2014) submitted to.
[41] N. Christofides, Graph Theory: An Algorithmic Approach, Academic Press, 1975.
[42] L. O. Chui, C. A. Desoer, E. S. Kuh, Linear and Nonlinear Circuits, McGraw-Hill, 1987.
[43] A. Kugi, Non-linear Control Based on Physical Models, Springer, 2001.
[44] A. Wu, P. Chapman, Simple expression for optimal current waveforms for permanent-magnet synchronous machine drives, IEEE Trans. Energy Convers. 20 (2005) 151–157.
[45] F. Baudart, E. Matagne, B. Dehez, F. Labrique, Optimal current waveforms for torque control of permanent magnet synchronous machines with any number of phases in open circuit, Mathematics and Computers in Simulation 90 (2013) 1–14.
[46] N. Lakshimi, B. Adhavan, V. Jagannathan, C. Ravichandran, Reduction of transient and steady state speed pulsation in permanent magnet synchronous motor using space vector pulse width modulation control, in: Proc. of the 2013 International Conference on Circuits, Power and Computing Technologies, Nagercoil, India, 2013, pp. 252–257.
[47] G. Sugimori, Y. Inoue, S. Morimoto, M. Sanada, Speed ripple reduction for an interior permanent-magnet synchronous motor based on sensorless voltage-current phase difference control, in: Proc. of the 5th International Symposium on Sensorless Control for Electrical Drives, Hiroshima, Japan, 2014, pp. 1–6.
[48] S. Li, C. Xia, X. Zhou, Disturbance rejection control method for permanent magnet synchronous motor speed-regulation system, Mechatronics 22 (2012) 7006–714.
[49] N. Vu, H. Choi, J. Jung, Certainty equivalence adaptive speed controller for permanent magnet synchronous motor, Mechatronics 22 (2012) 811–818.

Post-print version of the article: W. Kemmetmüller, D. Faustner, and A. Kugi, "Optimal torque control of permanent magnet synchronous machines using magnetic equivalent circuits", *Mechatronics*, vol. 32, pp. 22–33, 2015. DOI: 10.1016/j.mechatronics.2015.10.007
The content of this post-print version is identical to the published paper but without the publisher's final layout or copy editing.